RELAXATION TYPE OSCILLATIONS IN AN ARGON GLOW DISCHARGE

RICHARD J. STANSFIELD
AND
JOHN P. WISE

RELAXATION TYPE OSCILLATIONS IN AN ARGON GLOW DISCHARGE

* * * * * * * *

Richard J. Stansfield

and

John P. Wise

RELAXATION TYPE OSCILLATIONS IN AN ARGON GLOW DISCHARGE

by

Richard J. Stansfield

Lieutenant Commander, United States Navy

and

John P. Wise

Lieutenant Commander, United States Navy

Submitted in partial fulfillment of
the requirements for the degree of

MASTER OF SCIENCE
IN
PHYSICS

United States Naval Postgraduate School
Monterey, California

1 9 5 9

Frontispiece

RELAXATION TYPE OSCILLATIONS IN AN ARGON GLOW DISCHARGE

by

Richard J. Stansfield

and

John P. Wise

This work is accepted as fulfilling
the thesis requirements for the degree of
MASTER OF SCIENCE
IN
PHYSICS
from the
United States Naval Postgraduate School

ABSTRACT

Under certain conditions an anomalous mode exists in a medium pressure argon glow direct current discharge in which the entire positive column oscillates between minimum and maximum light intensity with a corresponding oscillation in voltage across the tube of very large amplitude. The conditions required to obtain the anomalous mode which proved to be a relaxation type oscillation were investigated and its characteristics ascertained.

Discharge times of the order of 10^{-5} seconds were obtained without using microwave techniques or equipment. An analysis was then made of the afterglow in argon at pressures between two and twenty mm of Hg. Afterglow decay processes appeared to follow those formulated by other investigators in that the decay processes were dependent upon the mode of external excitation of the gas and the gas pressure.

The writers wish to express their sincere thanks to Dr. N. L. Oleson for his keen interest and helpful guidance in the conduction of this investigation.

TABLE OF CONTENTS

LIST OF ILLUSTRATIONS

I

INTRODUCTION

During the investigation of moving and standing striations in the positive column of an argon glow discharge [1], plate resistances of the order of one megohm were placed in the circuit to complete the operating envelope of the tube. With these large resistances all normal modes were observed, but in addition there was an anomalous mode at low values of current (0.4 to 2.4 Ma).

The anomalous mode differed from the normal modes in two major aspects. First, peak to peak voltage oscillations across the tube increased from the order to 40 volts to the order of 500 volts. Second, striations previously termed moving (with velocities of about 200 meters per second) appeared in this mode to be pulsating or if moving to have velocities greater than 25,000 meters per second, the upper limit of the velocity measuring equipment. Reported evidence of previous observations of this anomalous mode could not be found.

In analyzing the anomalous mode, it was first necessary to determine its parameters: argon pressure, plate resistance, circuit capacitance, and electrode combination. Following this analysis an attempt was made to correlate the data obtained on discharge afterglow with that published by other investigators in this field. The variations of electron density as a function of time, mean electron decay time, and the increase in light intensity approximately 500 microseconds after end of discharge were of great enough significance to warrant an analysis.

II

APPARATUS AND EXPERIMENTAL TECHNIQUES

1. General

The apparatus employed in this study was originally designed by Dr. N. L. Oleson of the United States Naval Postgraduate School and built by Mr. I. C. Dumas of the Stanford Research Institute. It is the same as that used by McDonnel and Sherman [1] at the U. S. Naval Postgraduate School with the exception of the optical system. Fig. 1 is an overall schematic of the experimental set-up. Individual sections of the experimental set-up are discussed in the following paragraphs.

2. Discharge tube

Details of the discharge tube used throughout the study are shown in Fig. 2. A notable feature is the availability of several possible cathode-anode combinations. The molybdenum electrode consisted of an arrangement of four fins with an area of about 65 cm^2. The zirconium electrodes were solid right cylinders with an area of about 5 cm^2. The tube was mounted horizontally and connected through an Alpert valve [2] to a high vacuum system.

3. Vacuum and filling system

The vacuum system, as shown in Fig. 3, was simple in construction and provided an ultimate vacuum of 7×10^{-8} mm of Hg as measured with a VG-1A ion tube and Type DPA-38 ionization gauge, manufactured by Consolidated Vacuum Corporation. Filling with argon was accomplished in the manner evident from an inspection of Fig. 3 with the desired operating pressure observed on an oil manometer.

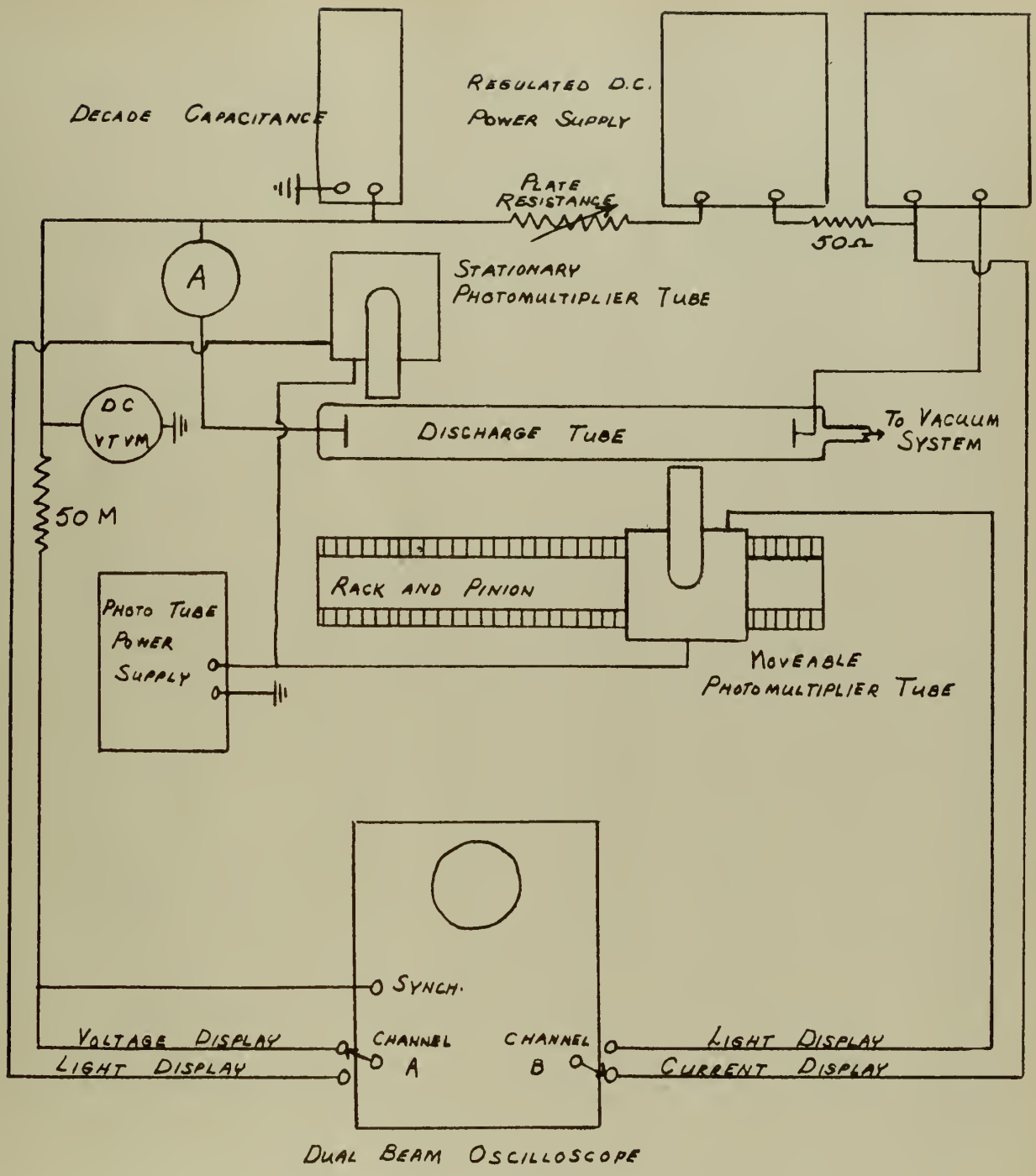

FIGURE 1

Overall Schematic Diagram of the Experimental Set-up

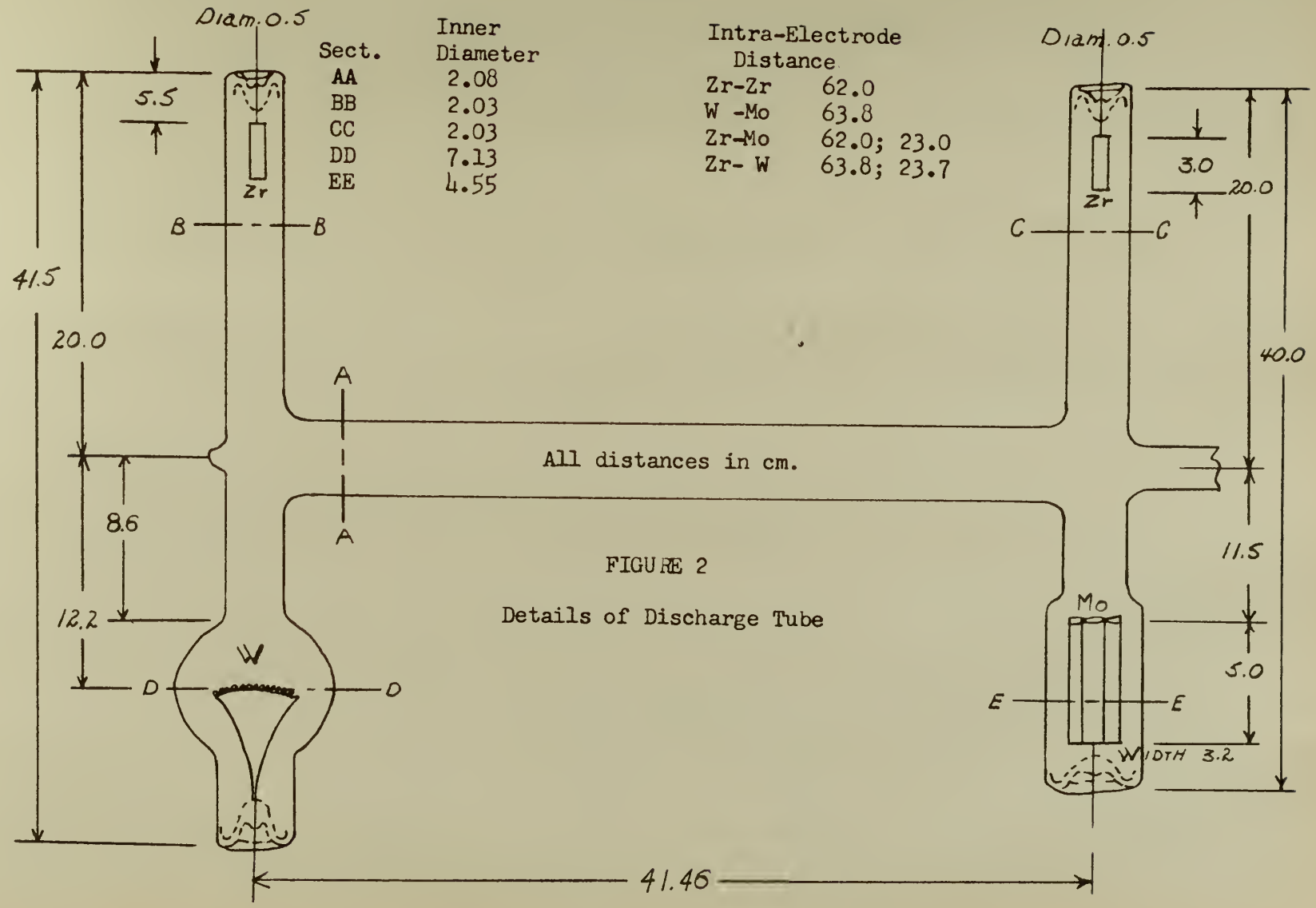

Sect.	Inner Diameter
AA	2.08
BB	2.03
CC	2.03
DD	7.13
EE	4.55

Intra-Electrode Distance	
Zr-Zr	62.0
W -Mo	63.8
Zr-Mo	62.0; 23.0
Zr- W	63.8; 23.7

All distances in cm.

FIGURE 2

Details of Discharge Tube

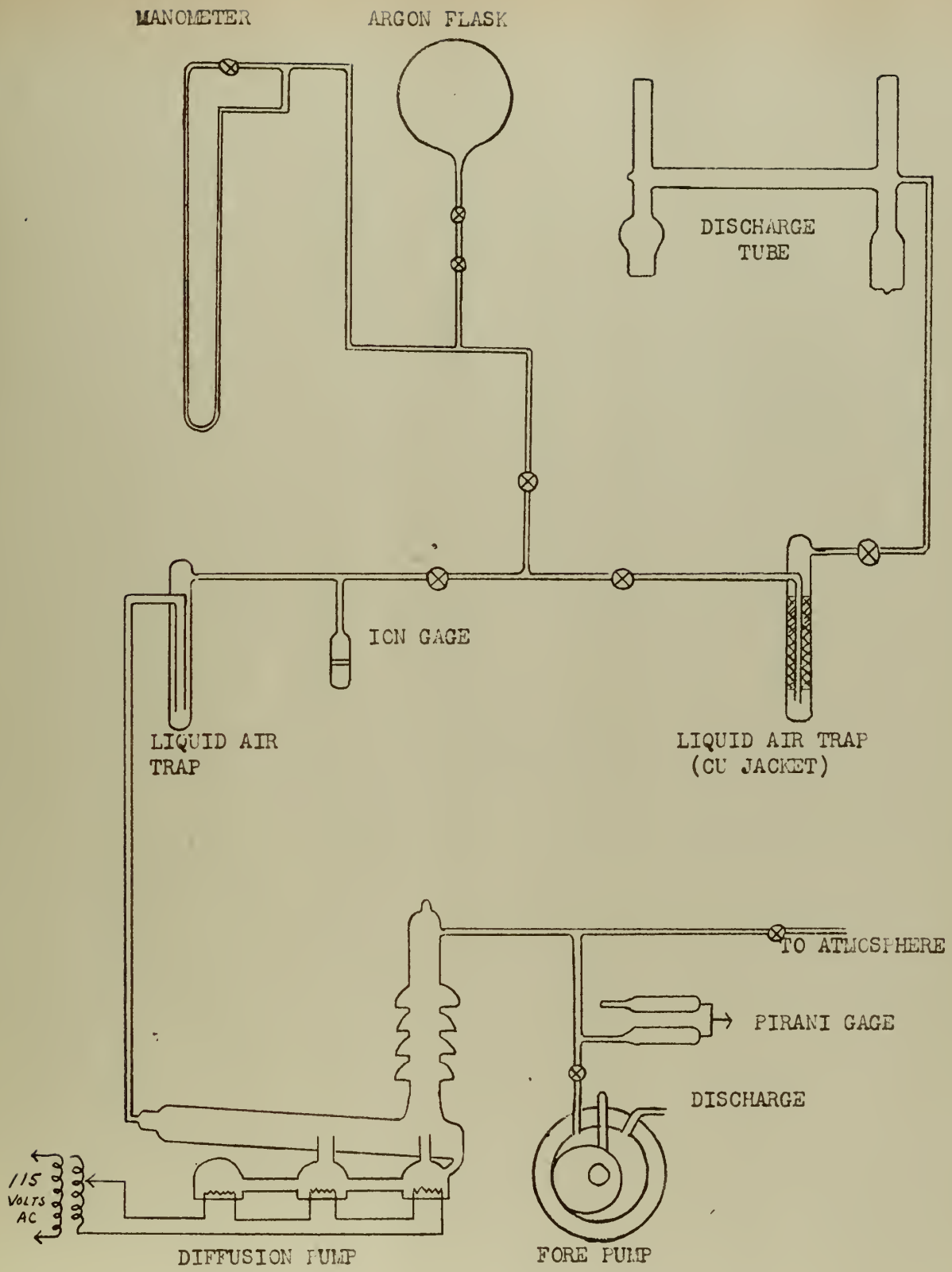

FIGURE 3

Schematic Diagram of Vacuum System

Considerable time and effort were expended to insure that the system was free from impurities. The following considerations and techniques were employed:

a. All glass stopcocks were lubricated with Apiezon N which has a vapor pressure of 10^{-8} to 10^{-9} mm of Hg at room temperature.

b. The manometer and the diffusion pump were filled with Octoil-S which has a vapor pressure of 5×10^{-9} mm of Hg at room temperature.

c. The discharge tube, the Alpert valve, and the glass tubing including the liquid air trap were degassed by baking for five hours at 400° C.

d. All electrodes were degassed by use of an induction heater for twenty minutes each followed by positive ion bombardment in the presence of argon.

e. The entire system was flamed using normal techniques.

f. Linde high purity ($1:10^{6}$) mass spectrometer controlled argon gas was fed through a liquid air trap at a very low rate to the discharge tube.

g. The discharge tube was isolated from the remainder of the system by means of an Alpert valve, as previously stated, and the remainder of the system maintained at high vacuum.

4. Optical system

Light from any point in the horizontal portion of the tube could be focused on the first photomultiplier tube mounted on the movable trolley on the optical rack and pinion carriage. The second photomultiplier tube could be permanently mounted at any given point along the horizontal column. The output of both photomultiplier tubes could be displayed on a dual-

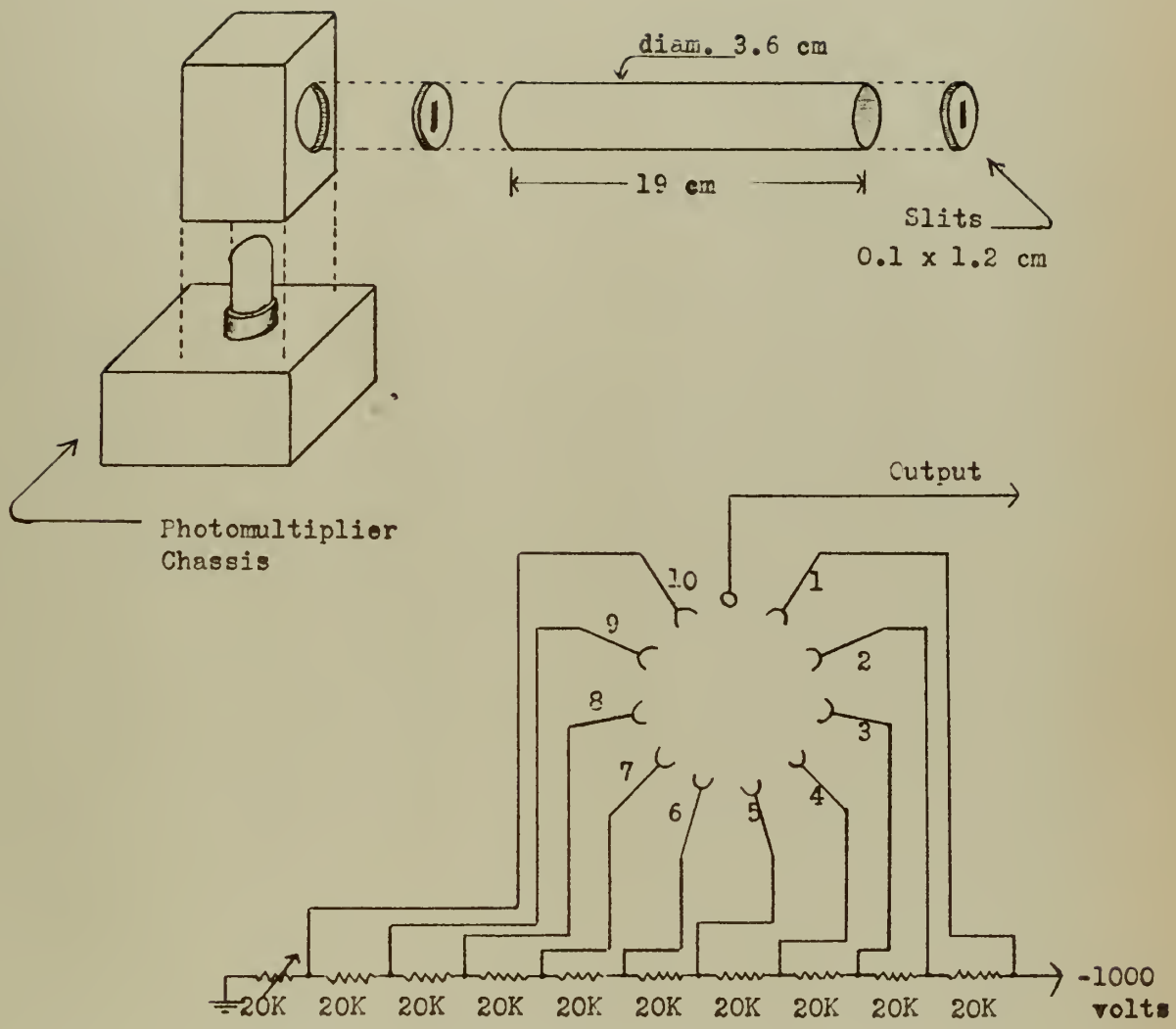

FIGURE 4

Sketch of optical system with photomultiplier circuit diagram.

beam oscilloscope, as could the voltage across the tube and the current through it. Thus a coincidence technique could be used to determine the velocity of any moving striations if such were present. Measurement of velocity up to 10^5 meters per second was possible with this technique. Fig. 4 is a sketch of the optical system and a circuit diagram of the photomultiplier.

Oscilloscope photography was accomplished with an oscilloscope record camera, type 299 using type 44 and type 40L film.

5. Circuitry and Instrumentation

The various circuits used in this study are discussed in the next section of this paper. The oscilloscope was calibrated for vertical and horizontal deflections.

6. List of Equipment

Dual Beam Cathode Ray Oscillograph, Hewlett-Packard, Model 150A

Frequency Counter, Hewlett-Packard, Model 524A

Oscillograph Record Camera, DuMont, Type 299

Ammeter, Weston Electrical Instrument Co. Model 931

Vacuum Tube Voltmeters, Hewlett-Packard, Model 410B

Photomultiplier Tubes, RCA 1P21, 1P22, 1P28

Photomultiplier Tube Power Supply, locally assembled

Power Supply, 1000V, Voltage Regulator, Kepco Labs, Model 1250B

Power Supply, 1500V, General Electric, Type YPD-4

Fore Pump, Central Scientific Co., Model HYVAC-7

Diffusion Pump, 2 stage, air cooled, Consolidated Vacuum Corp, Type GF-25A

Pirani Gauge, Distillation Products Inc., Type PG-1A

Ionization Gauge, Consolidated Vacuum Corp., Type DPA-38 with VG-1A ion tube

Induction Heater, Scientific Electric Co., Model AC-5-LB

Decade Condenser, General Radio Co., Type 219-M

III

CHARACTERISTICS OF THE ANOMALOUS MODE

1. General Observations

The discharge tube was filled with argon to a pressure of 2 mm Hg and connected to a 1400V regulated power supply through a variable resistance of 3 megohms. The upper left electrode (Fig. 2) of zirconium was used as cathode and the lower right electrode of molybdenum as anode giving a discharge path of 62 cm. in length. Voltage across the tube and the output of the movable photomultiplier tube were displayed on a dual beam oscilloscope.

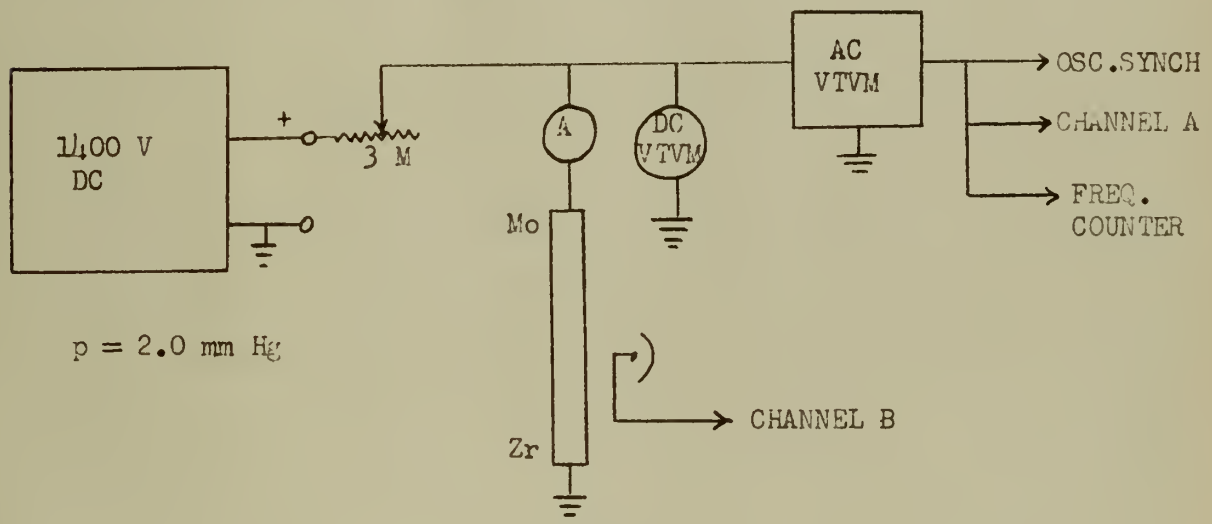

FIGURE 5

Circuit Diagram

The AC VTVM, shown in Fig. 5 had 11 megohm input impedance and provided an output signal at low impedance which was proportional to the input signal. It was found that the oscilloscope (1 megohm input impedance), when connected directly to the anode, loaded the discharge tube to the extent that oscillations in the anomalous mode could be sustained only at very low currents (0.4 to 0.5 ma.). Using the circuitry of Fig. 5 the

tube oscillated in the anomalous mode for all values of current between 0.4 and 1.2 ma. This range of currents corresponded to a resistance range of 2.52 megohm to 0.845 megohm. At higher currents the normal modes (moving striations) were observed.

2. Voltage and Frequency Characteristics

In the anomalous mode with circuitry as shown in Fig. 5 and at a pressure of 2 mm Hg the voltage across the tube was very nearly sinusoidal with a modulation of about 50%. This a-c voltage and its percentage modulation are shown in Fig. 6 as a function of current. The percentage modulation was computed using the equation

$$\% \text{ Mod.} = \frac{1}{2} \frac{(E_{MAX} - E_{MN})}{E_{d\text{-}c}} \times 100$$

The d-c voltage across the tube as measured by a DC VTVM decreased slowly with increasing d-c current as shown in Fig. 6 giving the tube a negative dynamic plate resistance. The instantaneous current through the tube was sinusoidal with the same percentage modulation as the voltage. The average current was read on a d-c ammeter. When operated in this region, the tube is not a passive circuit element but becomes an active element capable of supplying power to a load and supporting oscillations in a tuned circuit. Thus, in this region the tube may be classed as a negative resistance oscillator.

The frequency of oscillation increased nearly linearly with current as shown in Fig. 7. Frequency stability appeared to be excellent and no hysteresis effect was noted, i.e. a particular frequency could be obtained at a given current by an approach from a lower or higher current.

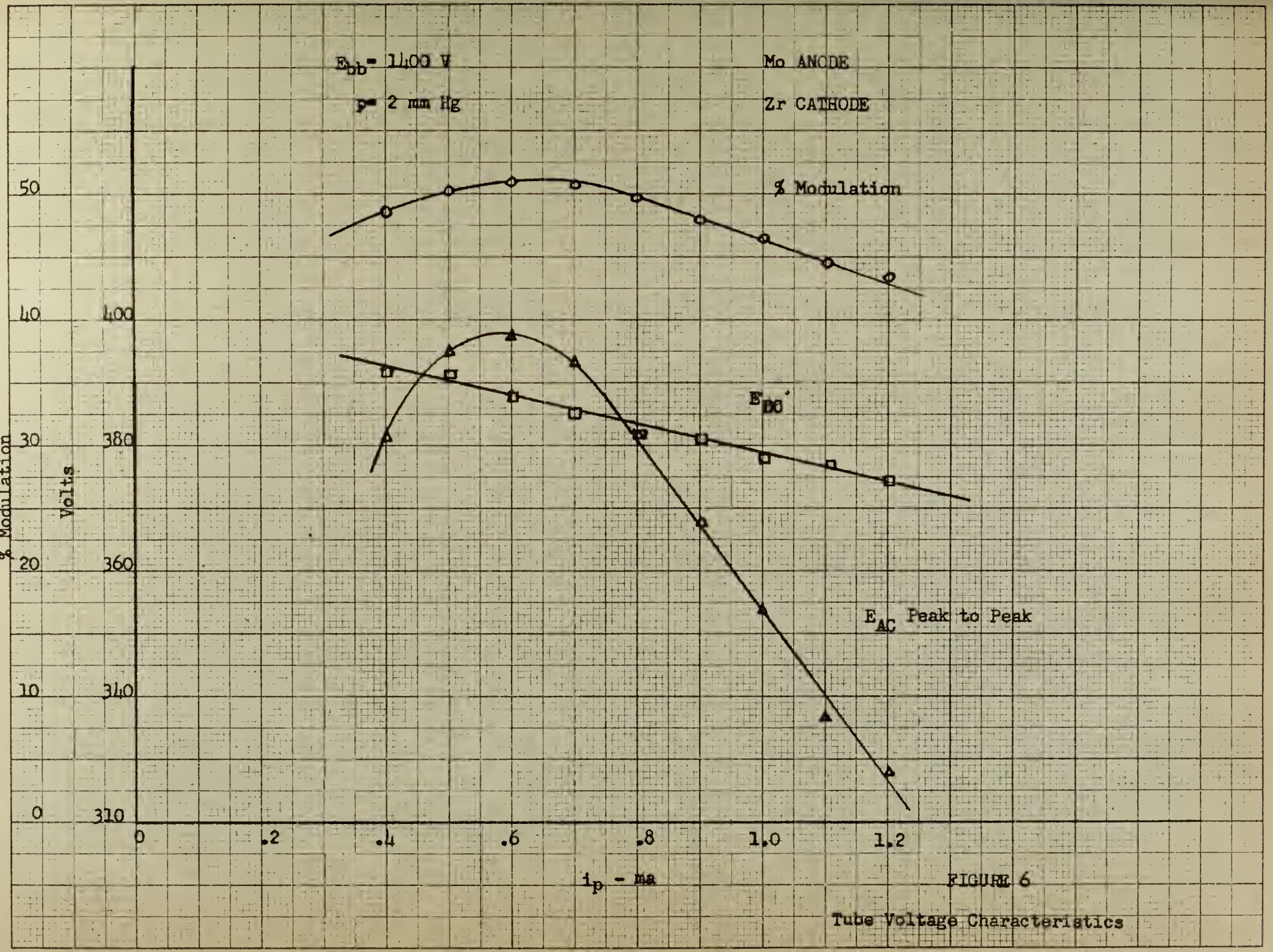

FIGURE 6

Tube Voltage Characteristics

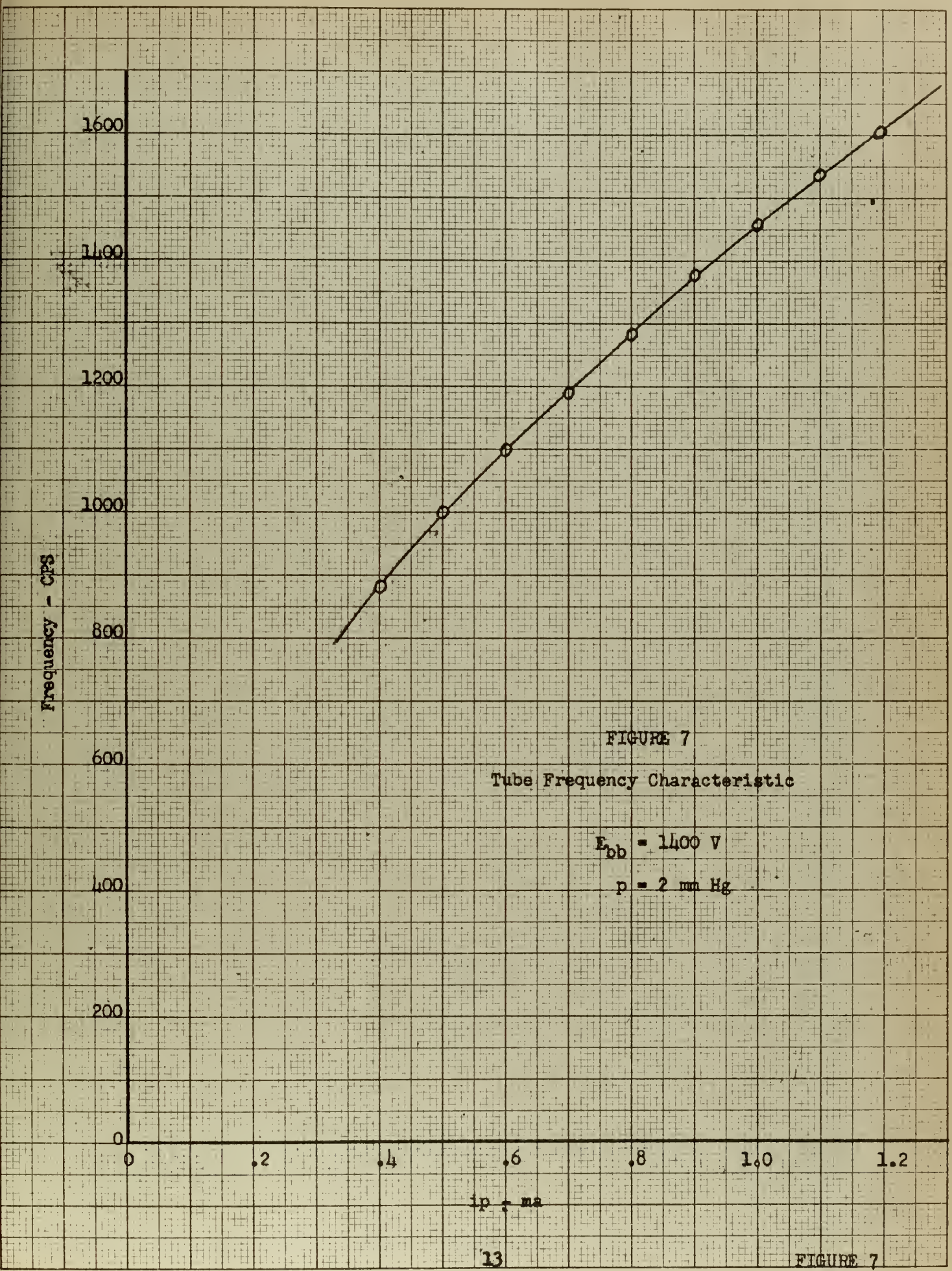

FIGURE 7

Tube Frequency Characteristic

E_{bb} = 1400 V

p = 2 mm Hg

FIGURE 7

The circuit resistance at any current is given by

$$R = \frac{1400 - E_{dc}}{i_p}$$

3. Capacitive Coupling

The oscilloscope was coupled to the anode through a 200 μμf capacitance with a 2000 μμf capacitance to ground with a measured insertion loss of 22.4 db as shown in Fig. 8. It was found that a resistance attenuator of less than 5 megohm input impedance quenched the oscillations. Peak to peak a-c voltage, percentage modulation, and d-c voltage across the tube are plotted in Fig. 9 as a function of d-c current. The tube again showed a negative dynamic resistance. Frequency was a linear function of d-c current as shown in Fig. 10. At d-c currents above 2.0 ma the normal modes (moving striations) appeared.

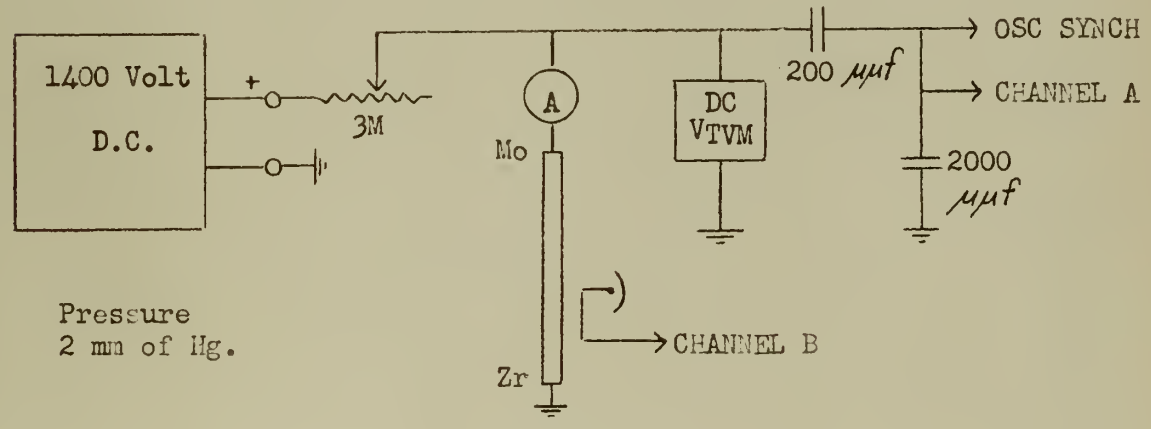

FIGURE 8

Circuit Diagram

4. Relaxation Oscillations

It was observed that small additional capacitance in parallel with stray capacitance increased the period of the oscillations. The oscillo-

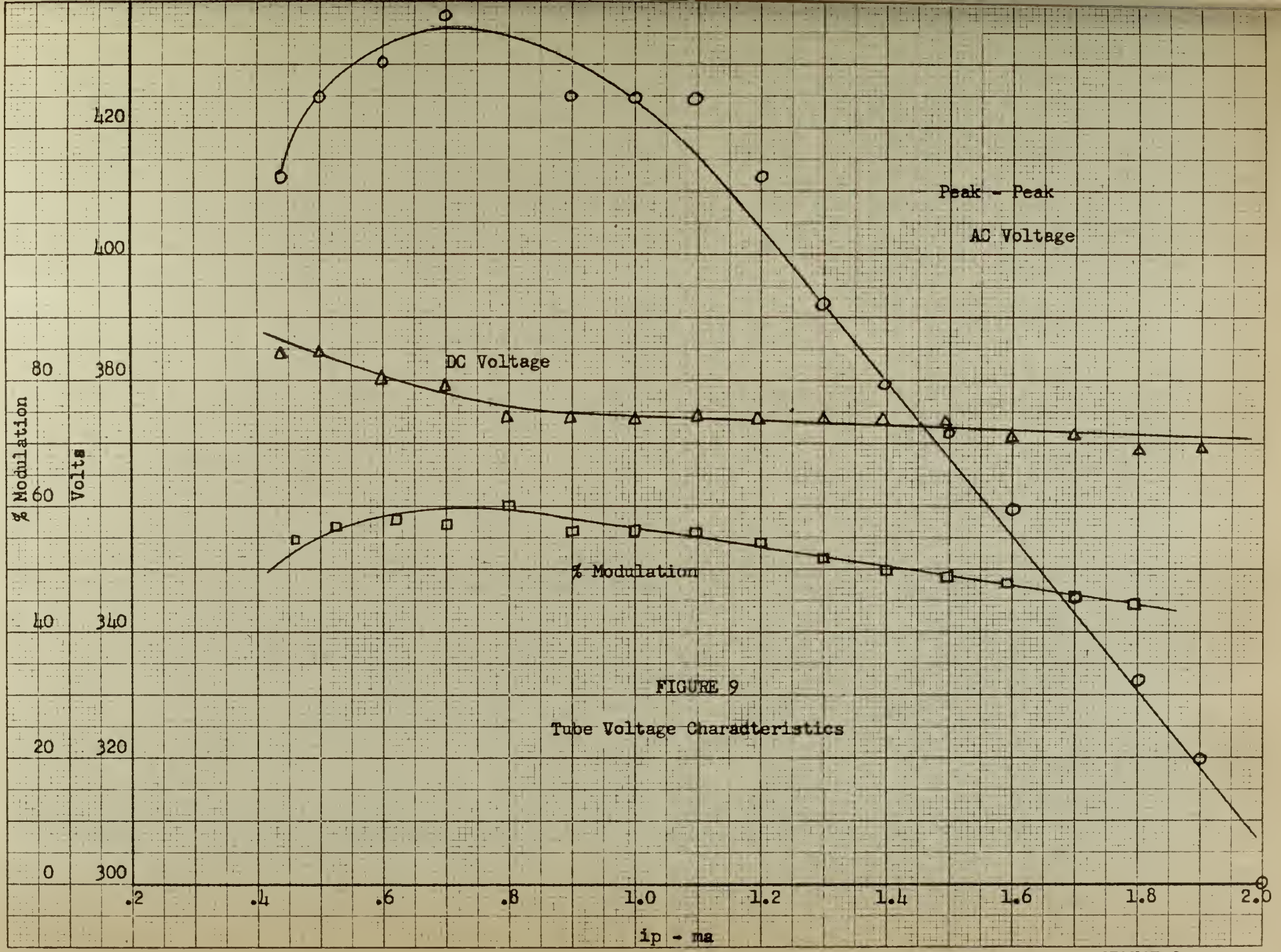

FIGURE 9

Tube Voltage Characteristics

FIGURE 9

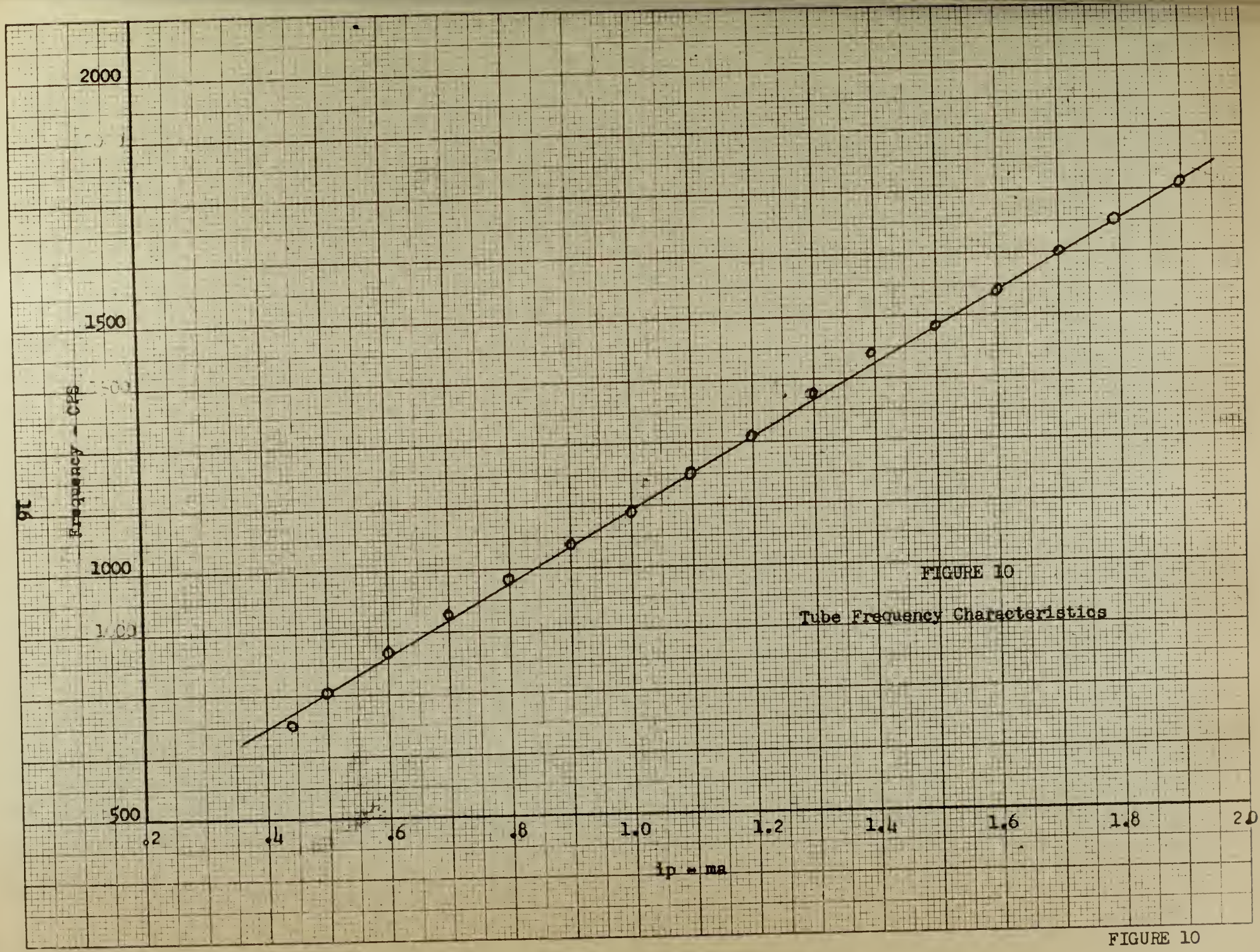

FIGURE 10

Tube Frequency Characteristics

FIGURE 10

scope was decoupled from the tube with a 50 megohm resistance and a variable capacitance to ground was connected as shown in Fig. 11. The stray capacitance to ground at the anode measured 1020 μμf. Signal attenuation through the 50 megohm resistor was 105:1.

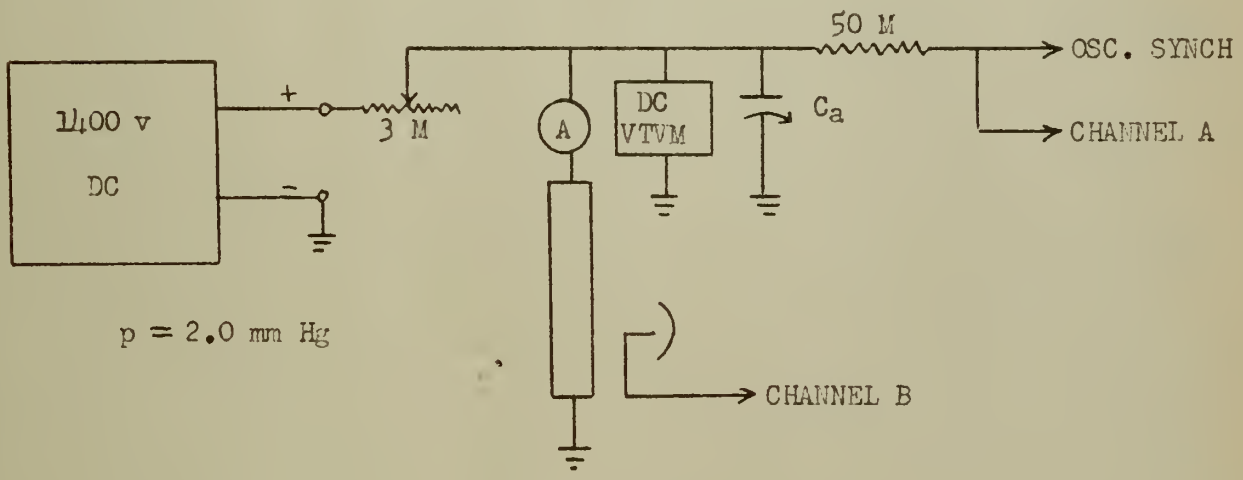

FIGURE 11

Circuit Diagram

The frequency was measured with a counter as both R and C_a were varied. Frequency was plotted on Fig. 12 as a function of the product RC where C is the sum of the stray capacitance and the additional capacitance. The empirical equation

$$f = \alpha (RC)^{\beta}$$

fits the curve very well. For the conditions of operation shown in Fig. 11 and with R in megohms, C in micro-microfarads, and f in cps:

$$\alpha = 92,500$$
$$\beta = -0.694$$

At very low values of RC, the voltage and the current waveforms were nearly sinusoidal. These waveforms degenerated as RC was increased with

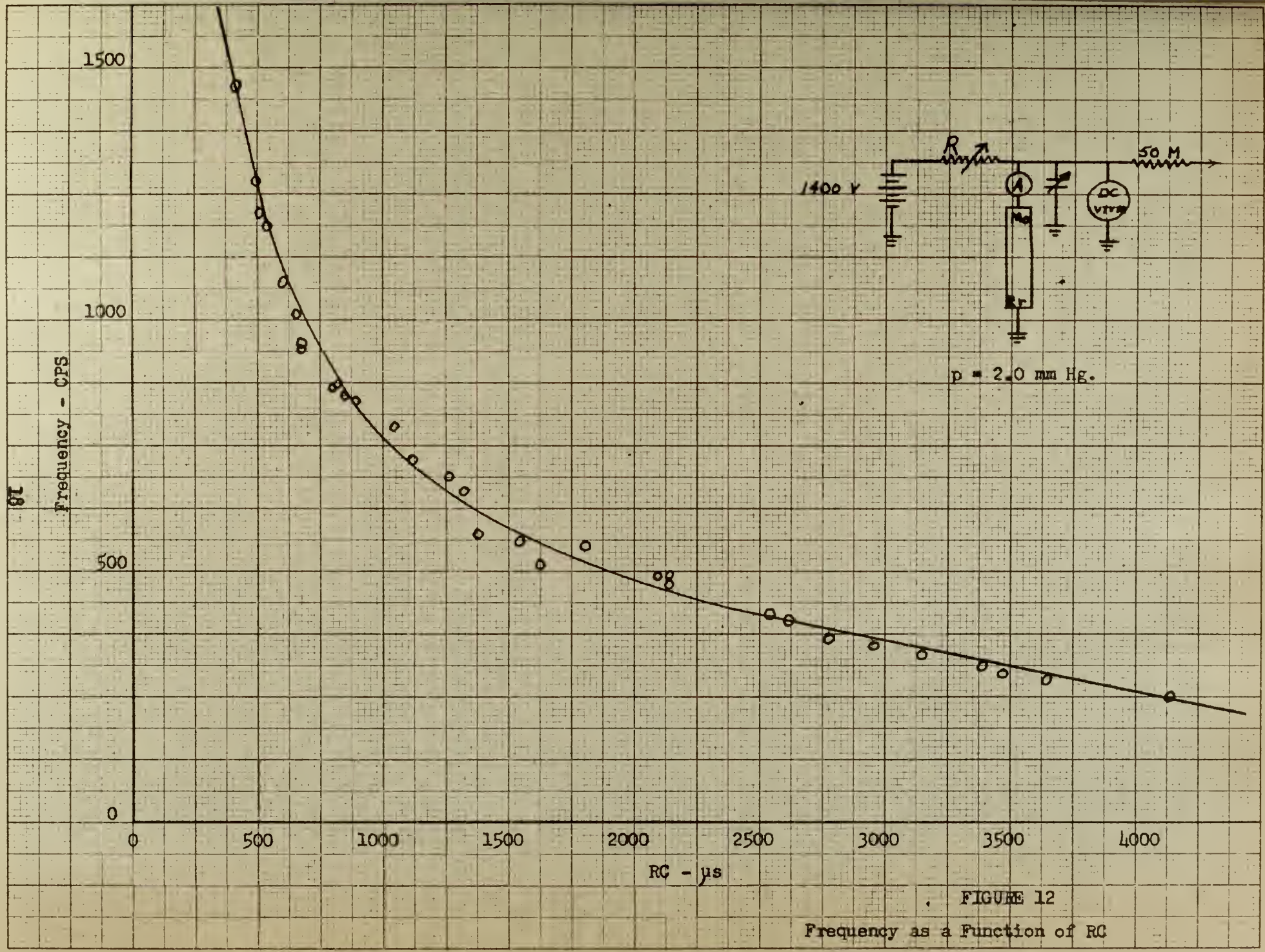

FIGURE 12

Frequency as a Function of RC

the voltage taking a sawtooth shape and the current becoming a sharp pulse. The current pulse occurred at the time when the voltage reached its maximum value. The tube exhibited a negative dynamic resistance throughout the range of RC and the tube operated as a relaxation oscillator except when RC was very low.

In a simple relaxation oscillator where the switching device can be assumed to operate instantaneously and to have zero resistance, the value of α will be a constant determined by the circuit parameters and β will be -1.

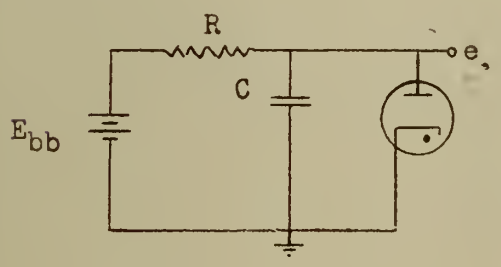

Relaxation Oscillator

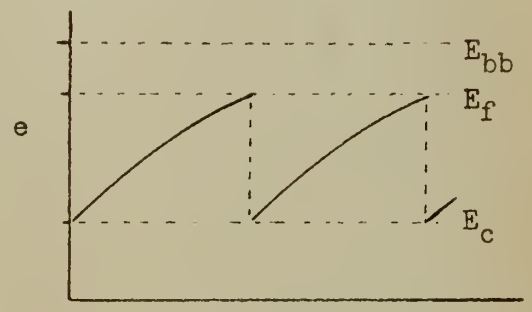

Let e = instantaneous voltage at anode
E_f = firing potential of switching device
E_c = cut off potential of switching device

The frequency of oscillation of the relaxation oscillator may be determined as follows:

$$E_f = E_c + (E_{bb} - E_c)(1 - e^{-T/RC})$$

Solving the equation for T,

$$T = RC \ln\left(\frac{E_{bb} - E_c}{E_{bb} - E_f}\right)$$

and the frequency is

$$f = \frac{1}{T} = \alpha(RC)^{\beta}$$

where

$$\alpha = \frac{1}{\ln\left(\frac{E_{bb} - E_s}{E_{bb} - E_f}\right)} \qquad \beta = -1$$

Analysis of the circuit as a conventional relaxation oscillator yields values for frequency of about twice that observed. GILL [3] reports that the period of these oscillations is a function of C+C' where C is the usual circuit capacitance and C' represents the effective self capacitance of the discharge. From another point of view, the negative dynamic resistance of the tube permits it to accept energy from the power supply during the charging of the external capacitance thus increasing its charging time. As a result the period of the oscillation is increased and the frequency is less than a conventional relaxation oscillator.

The effective self capacitance of the tube will be much larger than the geometrical capacitance of the electrodes in air because the plasma has a high dielectric constant and the effective distance between the electrodes is reduced by the length of the positive column since the voltage gradient along the positive column is nearly zero. The positive column was observed to extend to about 0.5 cm from the cathode and the cathode area was 5 cm^2. The capacitance is then:

$$C = 0.0885\ k\,(A/\ell)\ \mu\mu f$$

$$C = 0.885\ k\ \mu\mu f$$

where k is the dielectric constant of the plasma. In one calculation with the external capacitance equal to 2000 $\mu\mu f$, the value of C' was found to be 2200 $\mu\mu f$ giving k a value of 2.5×10^3.

5. Voltage, Current, and Light Waveform.

The range of the anomalous mode was extended to 25 ma d-c by the addition of capacity from anode to ground. The argon pressure was raised to 20 mm of Hg and the tube connected to 2500 volts as shown in Fig. 13.

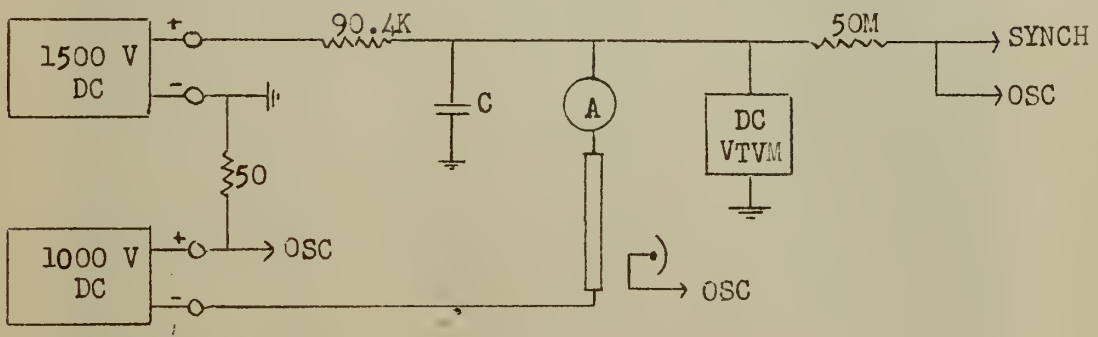

FIGURE 13

Circuit Diagram

Instantaneous tube current was measured by displaying on the oscilloscope the voltage across the 50 ohm precision resistor. Stray circuit capacitance to ground at the anode as measured by a capacitance bridge was 70 micromicrofarads. The value of the inserted capacitance was varied to yield values of RC between 284 and 1640 microseconds. Under these conditions the dynamic resistance of the tube was minus 95,000 ohms.

The sequence of oscillograms in Fig. 14 shows the voltage across the tube, the current through the tube, and the photomultiplier output voltage for various values of RC. It was noted that the period, voltage amplitude, and peak current increased with increasing RC. These together with peak light intensity for 20 mm of Hg are plotted in Fig. 17.

The current oscillograms showed that tube conduction occurred for only a few microseconds each cycle with current peaks of several amperes while

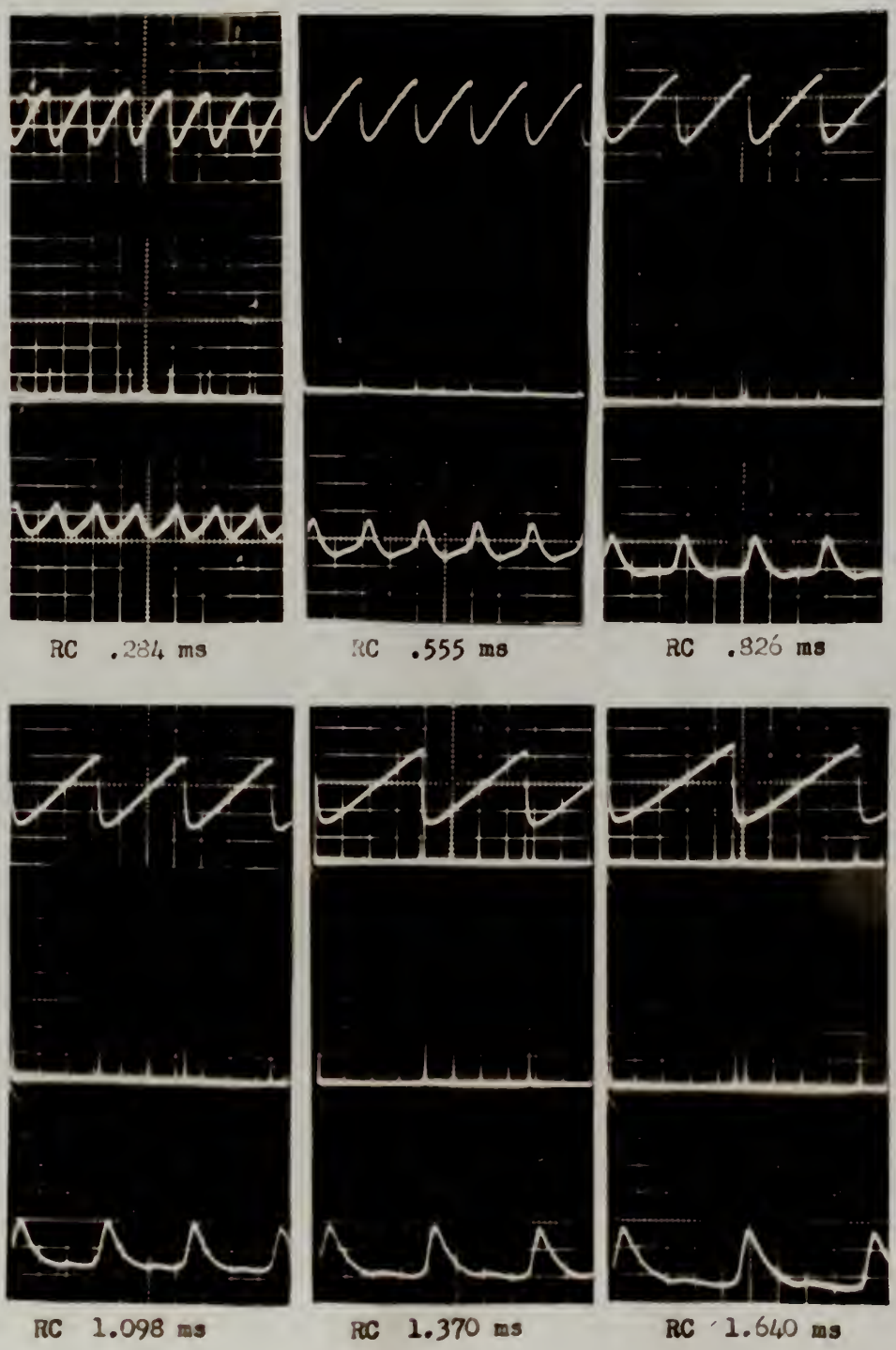

FIGURE 14

A sequence showing the voltage (top) at 530 volts/cm, the current at 400 ma/cm, and the photomultiplier output voltage (bottom) in arbitrary units above reference zero at bottom line. Reference zero current is bottom line. Time scale is 500 microseconds/cm. Pressure 20 mm of Hg.

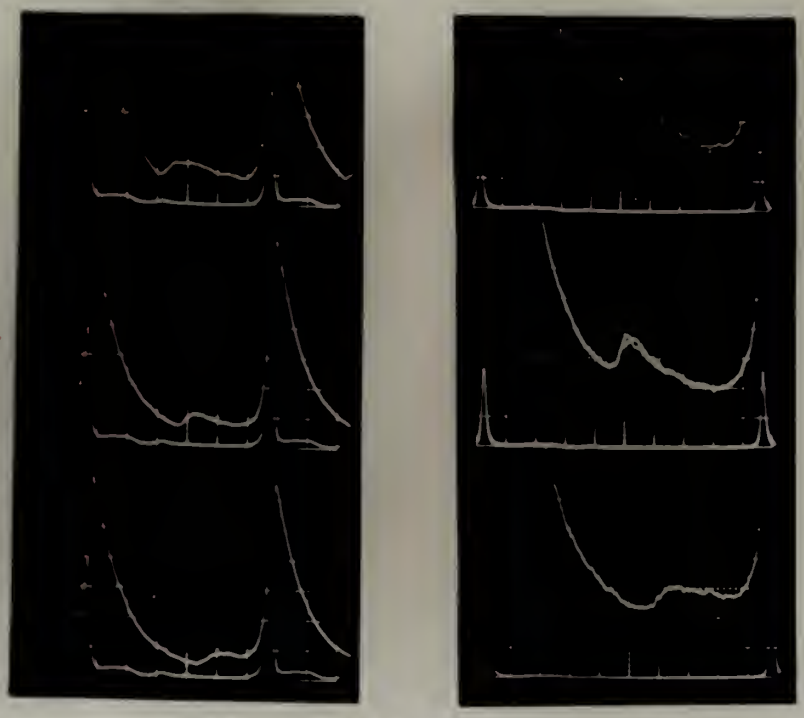

RC 4.08 ms RC 5.90 ms

FIGURE 15

Details of the afterglow on a time scale of 500 micro-seconds/cm, with the current superimposed for reference. Note that the smaller light peak occurs earlier as the contricted discharge moves nearer the wall under the influence of a magnetic field. Argon pressure 2.0 mm of Hg.

Current spike on a time scale of 5 micro-seconds/cm. Amplitude scale 400 ma/cm.
RC..... 2180 Micro-sec.
E_{bb} ... 2500 Volts
p ..... 13.5 mm of Hg

Oscillogram of light peak where the period is sufficiently long to permit complete decay; current on top trace for reference. Time scale is 500 micro-sec/cm.
RC ..... 2180 Micro-sec.
E_{bb} .... 2500 Volts
p ..... 8.3 mm of Hg.

Voltage at 530 V/cm, current at 500 ma/cm and light reference zero at minus one cm. Time scale is 200 Micro-seconds per cm.
RC ..... 1370 Micro-sec.
E_{bb} .... 2500 Volts
p ..... 11.8 mm of Hg.

FIGURE 16

Details of current spike and the afterglow.

FIGURE 17

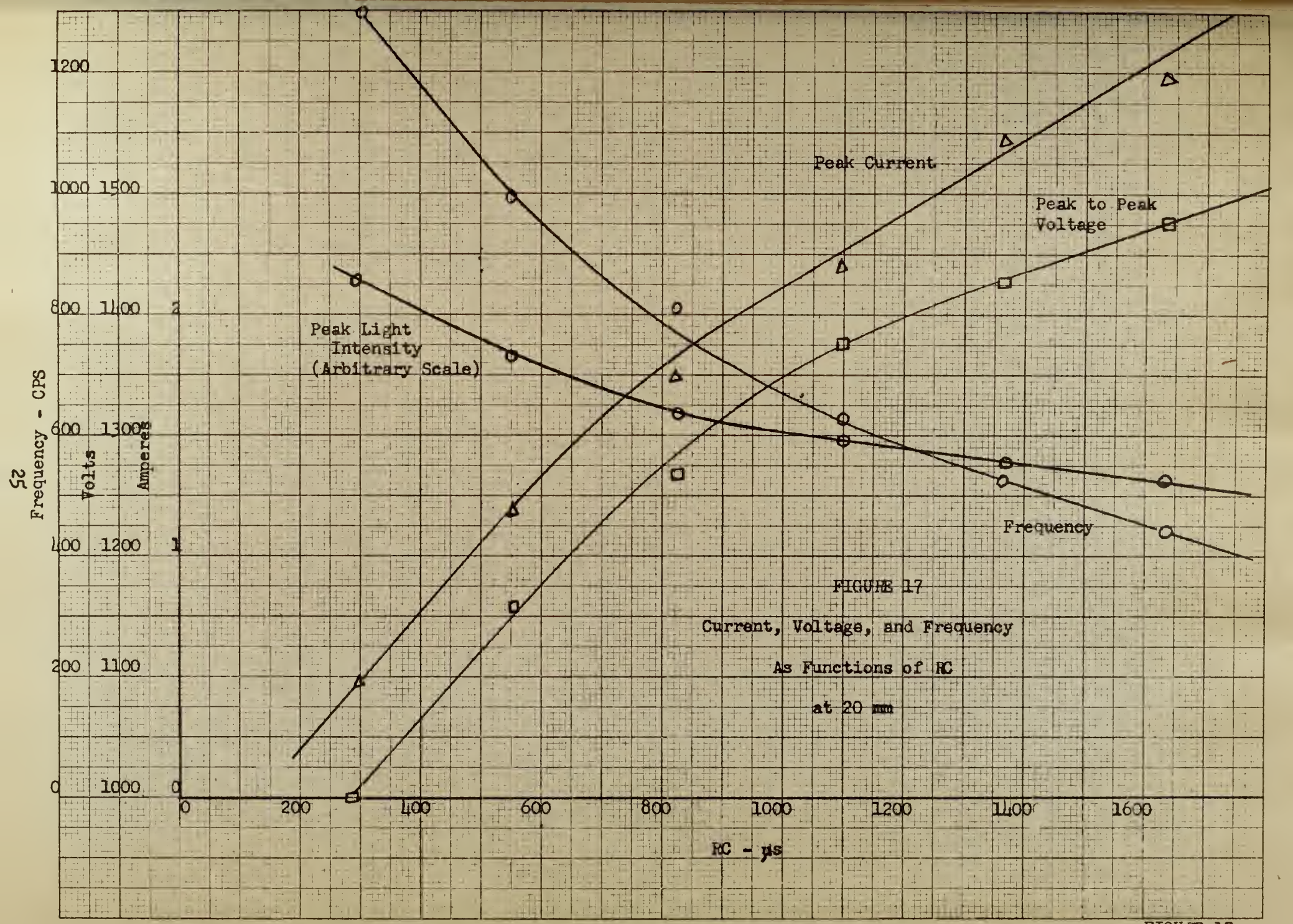

FIGURE 17

Current, Voltage, and Frequency

As Functions of RC

at 20 mm

FIGURE 17

the average tube current was only 20 ma. The width of the current pulse was about 10 microseconds. Integration under the pulse divided by the period gives an average value of current equal to the measured d-c value indicating that the current goes to zero between pulses. It was observed that the discharge constricted when the peak current was more than 400 ma so that it occupied only about 2% of the cross sectional area of the tube. The Faraday dark space appeared to be very short when the discharge was constricted, with the positive column extending up to within 0.5 cm of the cathode which was covered by the negative glow.

After the pulse of current, the light intensity built up rapidly to a maximum and then decayed. The processes responsible for this waveform are discussed in Section IV.

If the period between current pulses is short, the decay process is not completed between pulses and there will be cumulative ionization and excitation in the plasma. The percentage modulation of the light may be taken as an index of the average decay constant of the discharge. The percentage modulation as a function of the period is plotted on Fig. 18 for several values of pressure. These curves are extrapolated to 100% modulation to yield a characteristic decay time for the discharge. In the range of pressures from 6 to 20 mm of Hg the time required for extinction of the afterglow increased linearily with increasing pressure as shown on Fig. 18. This may indicate that diffusion to the walls is one mechanism by which metastable atoms are removed from the plasma inasmuch as diffusion time increases linearily with pressure.

It was found that a constricted discharge was obtained at argon pressures greater than 6 mm of Hg as shown on Fig. 19. At lower pressures the discharge was diffuse and occupied nearly the entire cross section of the

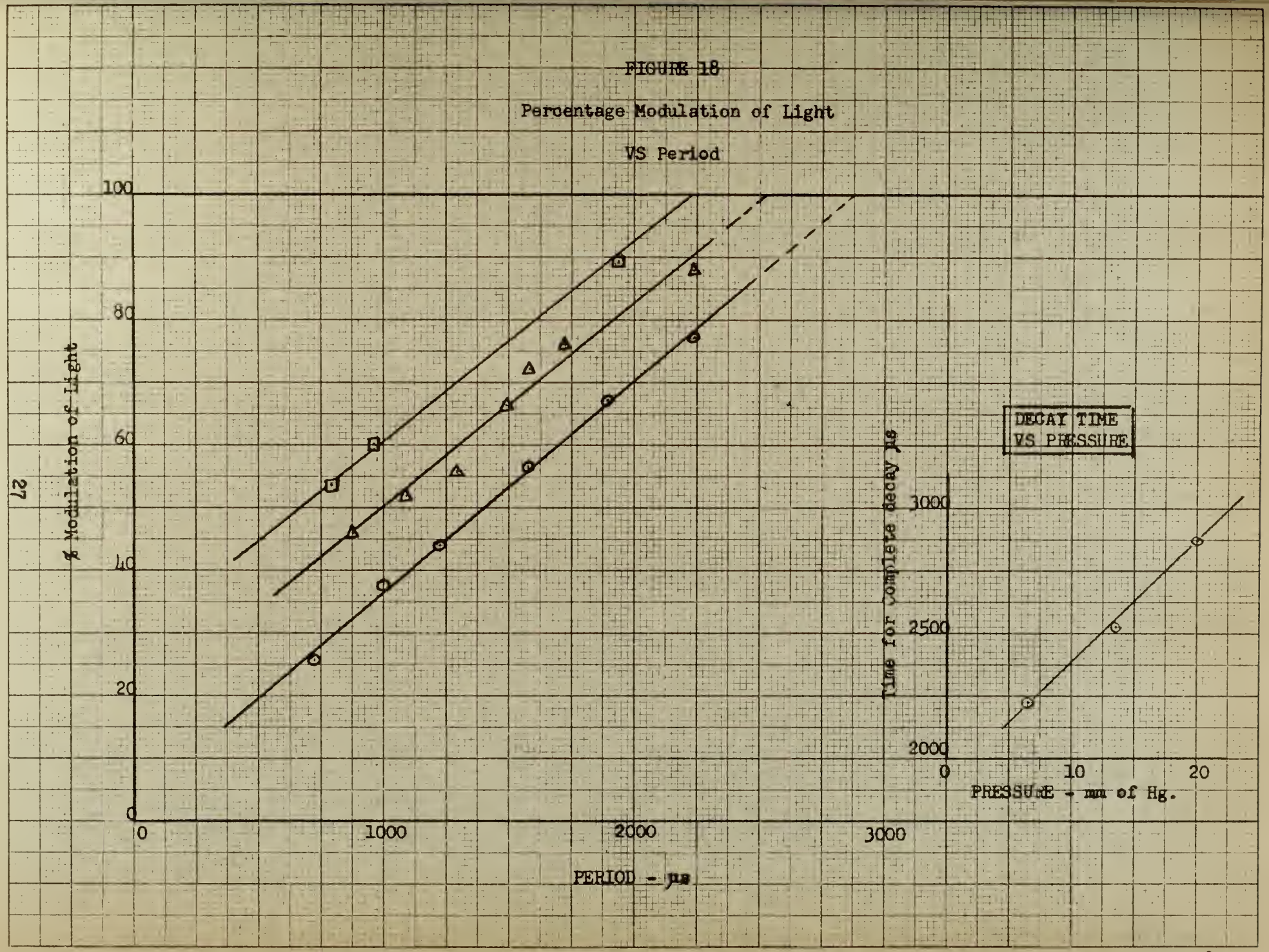
FIGURE 18
Percentage Modulation of Light
VS Period
% Modulation of Light
100
80
60
40
20
0
0
1000
2000
3000
PERIOD - µs
DECAY TIME
VS PRESSURE
Time for complete decay µs
3000
2500
2000
0
10
20
PRESSURE - mm of Hg.

FIGURE 18

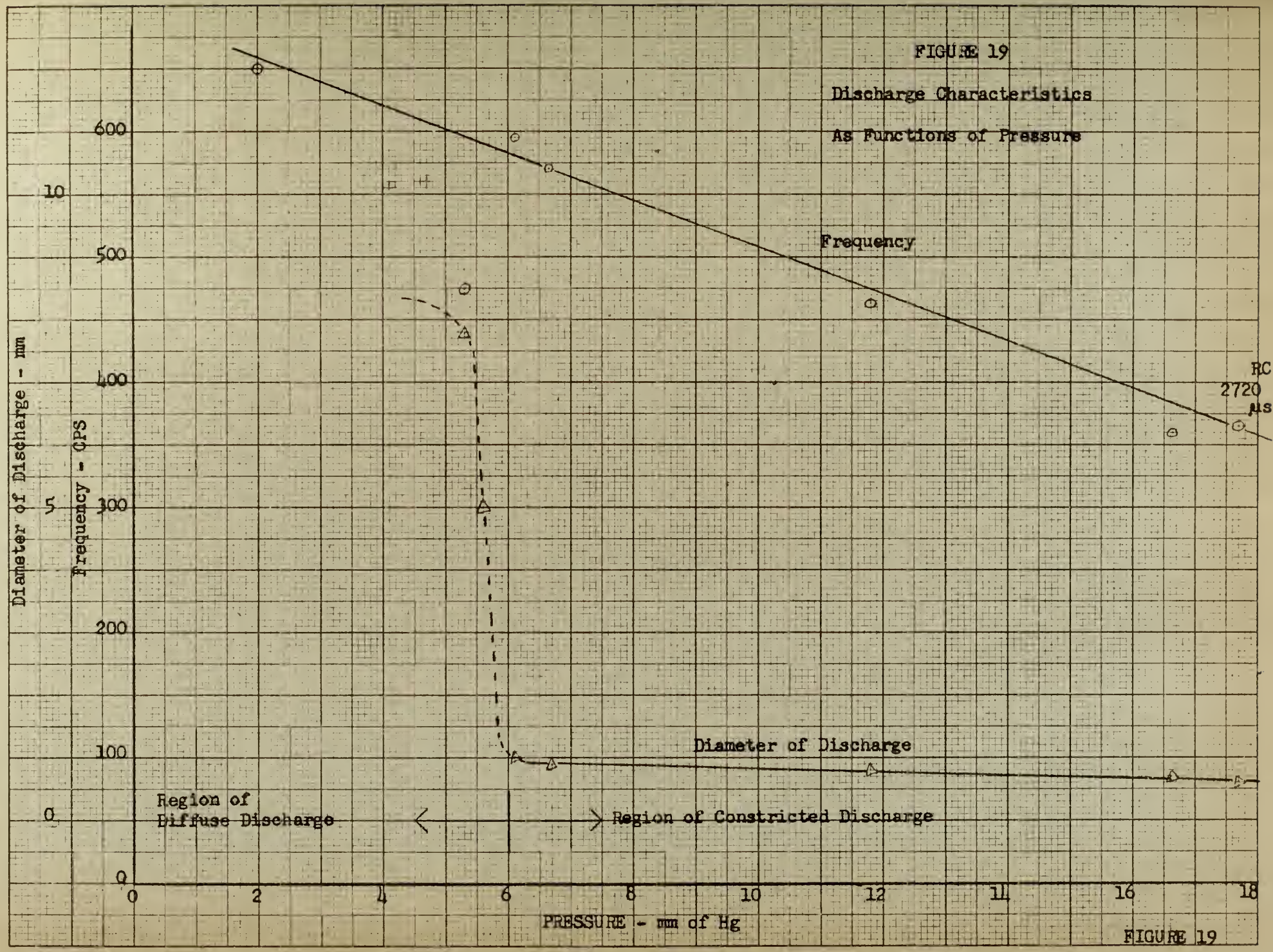
FIGURE 19
Discharge Characteristics
As Functions of Pressure
Frequency
RC
2720
µs
Diameter of Discharge
Region of
Diffuse Discharge
Region of Constricted Discharge
Diameter of Discharge - mm
Frequency - CPS
PRESSURE - mm of Hg
600
500
400
300
200
100
0
10
5
0
0
2
4
6
8
10
12
14
16
18

FIGURE 19

tube. The frequency of the oscillations at a constant RC product and E_{bb} decreased with increasing argon pressure as shown on Fig. 19. The voltage and current characteristics of the discharge tube in the range of pressures from 6 to 20 mm of Hg are plotted in Fig. 20. It is noted that the resistance of the discharge tube increases with increased argon pressure.

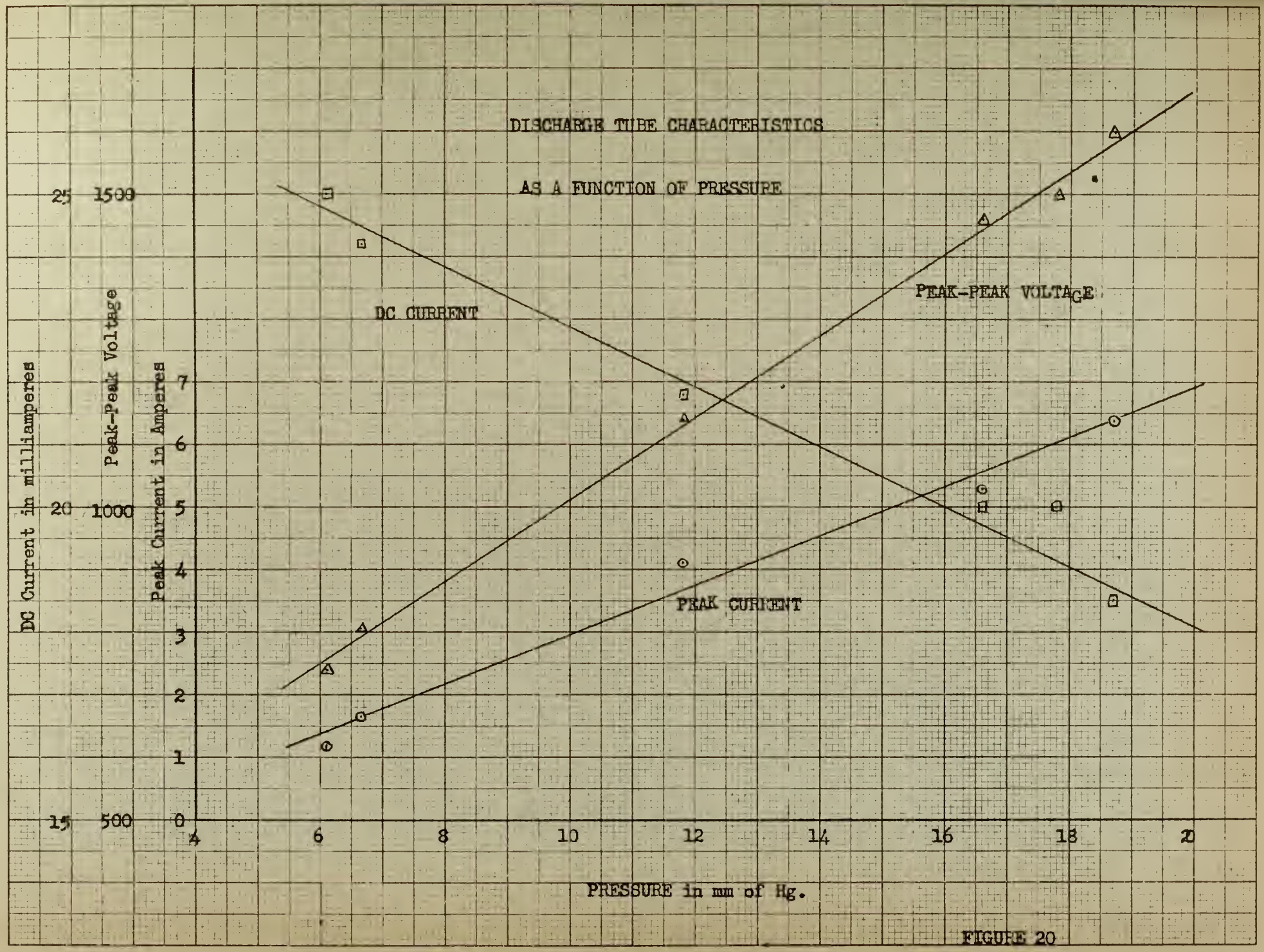
DISCHARGE TUBE CHARACTERISTICS
AS A FUNCTION OF PRESSURE
DC CURRENT
PEAK-PEAK VOLTAGE
PEAK CURRENT
DC Current in milliamperes
Peak-Peak Voltage
Peak Current in Amperes
PRESSURE in mm of Hg.
25
20
15
1500
1000
500
7
6
5
4
3
2
1
0
4
6
8
10
12
14
16
18
20

FIGURE 20

IV

STRUCTURE OF THE AFTERGLOW IN DECAYING GAS DISCHARGE PLASMA

1. General

It is now desirable to discuss those processes by which radiant energy in the visible spectrum is emitted, the processes leading to this emission, and then to relate quantitatively the results of this study to other reported studies.

After removal of the applied field from a gaseous discharge plasma, the "abandoned" plasma evolves and decays. In the absence of further excitation the gas would eventually reach its original non-excited normal state determined by the d-c supply voltage and series resistance. The duration of this evolution depends upon the geometry of the gas container, the nature of the gas, gas pressure, and the conditions of excitation. [4]. Since the same gas, argon, and the same discharge tube were used throughout this study, dependence on these factors was accepted. Dependence on the conditions of excitation was amply demonstrated in the previous section by the writers and is seen in Figs. 14, 15, and 16.

During excitation, the plasma stores energy gained from the applied field and this energy is recovered during the plasma decay. Kinetic energy is stored as thermal energy of electrons, positive ions, and normal atoms; potential energy is stored by excited and metastable atoms. It is therefore expected that the plasma could remain active for a short time, even after the means of excitation had been removed. For purposes of analysis, the afterglow period is divided into the early and late phases.

2. Early Afterglow Excitation and Decay

Due to high energy electrons produced in the early stages of plasma build up and possibly to the action of metastables [5], ionization and excitation will continue for a while after the applied field is cut off. Continued thermal ionization as electron temperature decreases, along with a reduction in the rate of removal of charges results in an increase in ion and electron density. A point in time is finally reached where the rate of ionization is just equal to the rate of removal of ions and electrons by recombination (a minor contribution at higher electron temperatures) and diffusion to the walls. This point represents the peak of the light intensity curve and, in agreement with theory [6], is observed to occur about 100 microseconds after the peak current as seen in Figs. 14, 15, and 16.

It is to be observed that light is at its minimum value for approximately 3000 microseconds during which time no moving striations are observed in the photograph. From measurements of moving striations in argon [1], their velocities are from 100 to 400 meters per second. Hence if we take into account the anode-cathode distance, 62 cm., and assuming a striation velocity of 200 meters per second, the striation should travel from the cathode to the anode in approximately 3.1 ms. But current is zero during this time and no travelling striation should be observed.

Electron temperature decrease is due to two processes:

a. Elastic collision of electrons with atoms in their ground state.

b. Inelastic collision of electrons with metastable atoms with re-

sulting cumulative excitation.

The electron temperature must be below the ionization potential of the atom for both of these processes. Inelastic collisions between electrons and excited atoms are not considered since excited atoms have a mean-life of only about 10^{-9} seconds.

3. Late Afterglow Decay

In the late afterglow phases, the decreasing light intensity observed may be attributed to four primary processes which spectographically produce both an arc line spectrum and a continuum. Recombination of electrons and ions accounts for a large fraction of the arc line intensity although it amounts to only a few percent of the total radiation from the plasma. The intense continuum, accounting for most of the emitted radiation, is primarily due to retardation of electrons moving in orbits about ions ("free-free" transitions). The rate of decay of this bremsstrahlung radiation depends both on the rate of decrease of plasma ion density and the rate at which the mean energy of the electrons is diminishing [7]. Contrary to this, preliminary measurements by Booth and Albers indicate little or no continuum in the visible region, indicating this process plays no part. The third electron density decay process is by diffusion to the walls. The fourth process is metastable atom diffusion which becomes noticeably paramount at the end of the later phase of decay. This process is quantitatively discussed in the next section of this paper.

4. Quantitative Comparisons

Quantitative comparisons in this study are of necessity very circumspect due to lack of a means of measuring ion or electron density directly.

Attempts made to use the spare zirconium electrode as a probe were completely unsuccessful.

The recombination process in plasmas is described by

$$\frac{dN_+}{dt} = \frac{dN_e}{dt} = -\alpha N_+ N_e = -\alpha N_e^2$$

where α is the recombination coefficient [7]. If N_1 and N_2 are the electron densities at times t_1 and t_2, respectively,

$$\frac{1}{N_2} - \frac{1}{N_1} = \alpha (t_2 - t_1)$$

Light intensity is related to electron density by

$$I = k N_e^2$$

where k is the proportionality constant. Thus

$$\frac{1}{I_2^{1/2}} - \frac{1}{I_1^{1/2}} = k^{-1/2} \alpha (t_2 - t_1)$$

Fig. 21 is a plot of this relation, assuming a value for α and measuring intensity as a function of time after end of discharge. From this information k can be determined and then electron density as a function of time. These values are shown in Fig. 22, the customary plot of 1/N vs t. The slope of this curve is the assumed α and is seen to be independent of pressure as was found by Biondi and Brown [8]. Redfield and Holt [4] attribute the flattening out of curves similar to Fig. 21 to the fluorescence effect of the quartz glass discharge tube.

The electron density decay, when both ambipolar diffusion and recombination are the operating removal processes is

$$-\frac{\partial N_e}{\partial t} = \alpha N_e^2 + D_a \nabla^2 N_e$$

where α is the recombination coefficient, D_a the ambipolar diffusion coefficient, and N_e is the electron density as a function of space and time. Redfield and Holt [4] solved the equation as

$$-\frac{dN_e}{dt} = 0.54\,\alpha N_e^2 + \frac{N_e}{\tau}$$

by assuming that spatial distribution of electrons which did not perturb their solution. Biondi and Brown [6] assumed a density of electrons equal to the average density and solved the equation as

$$-\frac{dN_e}{dt} = 0.27\,\alpha N_e^2 + \frac{N_e}{\tau}$$

In both solutions N_e = const x exp $(-t/\tau)$ where τ is the time constant associated with an exponential decay of the electron density. From Fig. 21 and the above equation a value of τ was calculated.

Other researchers in this field have determined values of α by two separate techniques, probes and microwaves. Earlier work [9] using probe techniques after the cutoff of a direct current discharge gave values of about 2×10^{-10} cm^3/ion-sec for α, but with low probable accuracy owing to a number of uncertainties in the measurements, the nature of which are discussed in the original paper. Recent work [10] with the use of double probes rather than a single one for following plasma decays makes it clear that it is necessary to be very careful in the interpretation of single probe measurements after excitation has been removed.

Two independent groups of researchers [4,8] using microwave techniques determined the value of the recombination coefficient at the relatively high pressures used in the present investigation to be about 3×10^{-7} cm^3/ion-sec. Bates [11] proposed that in the monatomic rare

gases the electrons recombine with molecular ions rather than atomic ions and part of the available energy in the system of positive ions and electrons is used up in the dissociation of molecular ions. It has been shown that formation of molecular ions requires less energy than the formation of an atomic ion, 0.7 ev less for argon [7], and that molecular ions are probably formed by a two stage process involving first excitation and then collision of the excited atom with a neutral atom.

$$A + h\nu \longrightarrow A^*$$
$$A^* + A \longrightarrow A_2^+ + e^-$$

The results of the experiments of Biondi [12] lend very strong support to the validity of Bates' proposal, according to which the large recombination coefficients ($\sim 10^{-7}$) measured in monatomic rare gases are to be ascribed to thermal electron recombinations with molecular ions. Such recombinations are followed by dissociation of these molecules into atoms, of which at least one is in an excited state that decays with radiation, giving rise to the recombination afterglow.

$$A_2^+ + e^- \longrightarrow A^* + A$$
$$A^* \longrightarrow A + h\nu$$

The writers accepted this later value as being the most accurate one determined to date most nearly fulfilling the conditions of geometry, mode of excitation, type of gas, and gas pressure used in this study. Thus with α assumed to be 3×10^{-7} cm^3/ion-sec, ion densities of the order of $10^9/cm^3$ and characteristic calculated decay times of the order of 10^{-4} seconds were obtained. Both values are in good agreement with reported values [4,8].

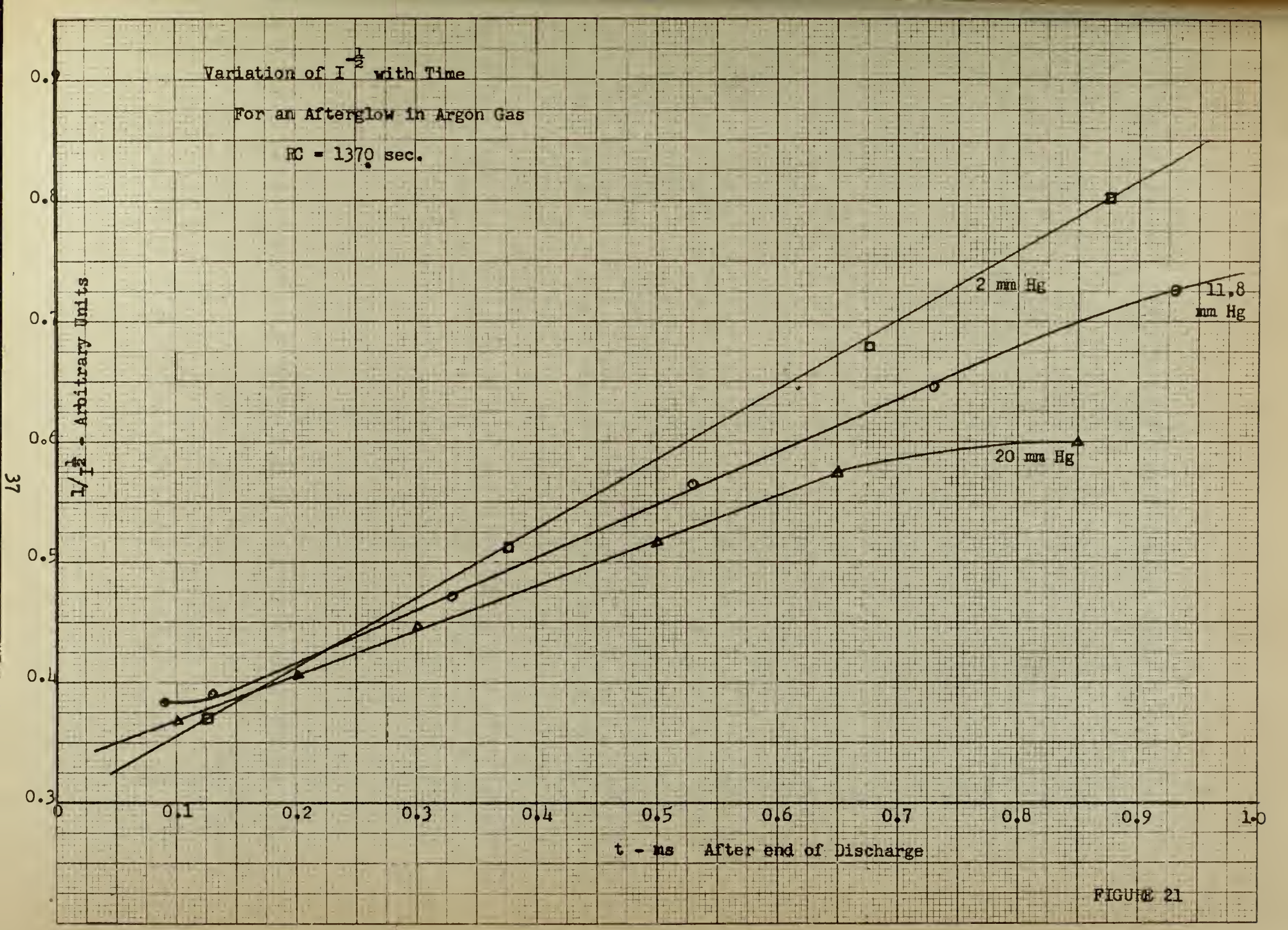
Variation of $I^{-\frac{1}{2}}$ with Time
For an Afterglow in Argon Gas
RC = 1370 sec.
$1/I^{\frac{1}{2}}$ - Arbitrary Units
2 mm Hg
11.8 mm Hg
20 mm Hg
0.3
0.4
0.5
0.6
0.7
0.8
0.9
0
0.1
0.2
0.3
0.4
0.5
0.6
0.7
0.8
0.9
1.0
t - ms After end of Discharge

FIGURE 21

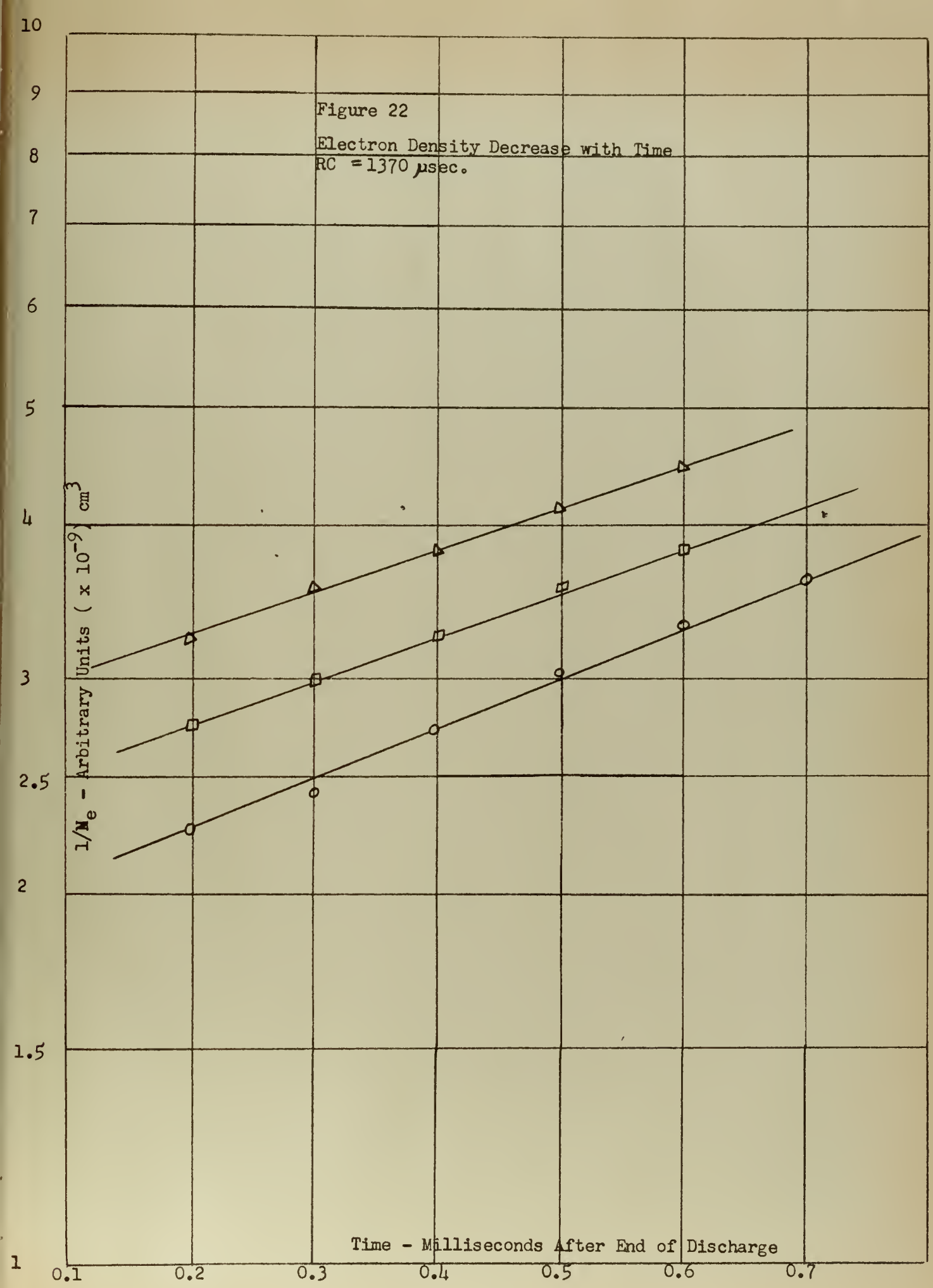
Figure 22
Electron Density Decrease with Time
RC = 1370 μsec.
1/Ne - Arbitrary Units (x 10^-9) cm^3
Time - Milliseconds After End of Discharge
10
9
8
7
6
5
4
3
2.5
2
1.5
1
0.1
0.2
0.3
0.4
0.5
0.6
0.7

V

THE SECONDARY LIGHT PEAK

1. Theory of Origin.

During the later part of the afterglow there appeared a small increase in light intensity. This secondary light peak is believed due to diffusion of argon metastable atoms to the walls where they lose their excess energy by radiation. After excitation has ceased, metastable atoms are removed from the discharge principally by collision with neutrals or diffusion to the walls. [13].

A collision with a neutral of sufficient energy will raise a metastable atom to a radiative state from which it will go to the ground state in about 10^{-8} seconds. The velocity distribution of neutrals at the temperature of the discharge ($300^{\circ}K$) permits a few to have energies high enough to make the process very likely. The probability of the process has been estimated by Colli [14] as one in 2×10^{5} impacts. According to Molnar [15], the collision cross section for metastable argon atoms is 6.35 times that for neutral argon atoms. The collision frequency of the metastable atoms at $300^{\circ}K$ and 11.8 mm of Hg is then 5.5×10^{8} sec^{-1} and the mean life is 0.36×10^{-3} seconds.

The value of the diffusion constant for argon metastables at 1 mm pressure at $25^{\circ}C$ is given by Loeb [15] as 45 ± 4 cm^2/sec. At other pressures

$$D = D_o \left(\frac{p_o}{p} \right)$$

if the temperature is constant. The value of the diffusion constant so computed is 3.8 cm^2/sec at 11.8 mm of Hg. If it is assumed that metas-

table atoms are formed in the discharge during the current pulse only and diffuse outward, then at a radial distance r, the density of metastables at a time t is given by [10]

$$n_r = \frac{n_o}{(4\pi D t)^{3/2}} e^{-\frac{r^2}{4Dt}}$$

where n_o is the number of metastables per unit volume at the center at the end of the current pulse which is taken as the zero of time. However, the total number of metastable atoms is being reduced with time by collisions with neutrals so that

$$N = N_o e^{-\frac{t}{\tau}}$$

where

$$N = nV$$

Therefore the fraction of the total number of metastables formed appearing at the wall is

$$\frac{N_{r_o}}{N_o} = \frac{e^{-\frac{t}{\tau}}}{(4\pi D t)^{3/2}} e^{-\frac{r_o^2}{4Dt}}$$

This function is zero at t = 0 and at t = ∞ and rises to a maximum at

$$t = -\frac{3\tau}{4} + \frac{1}{2}\sqrt{\frac{9\tau^2}{4} + \frac{r_o^2 \tau}{D}}$$

2. Quantitative Comparisons.

The distance from the constricted discharge to the wall of the tube was varied by the application of a small magnetic field. Since the required magnetic field was very small it is believed that it had a negli-

gible effect on the processes occurring in the discharge. The distance from the periphery of the discharge to the inside surface of the wall and the diameter of the discharge were measured with a cathometer. The distance, r_o, from the discharge to the wall was obtained as shown below, where πr_1^2 is one half the total area of the discharge.

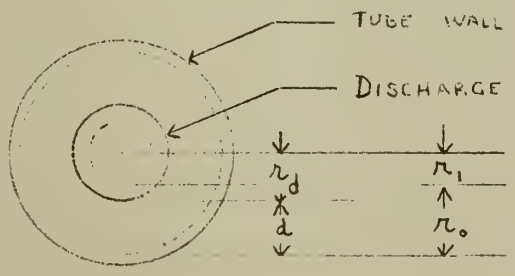

$$r_o = d + .293 r_d$$

It was found that the time of arrival of the secondary light peak increased linearily with distance as shown on Fig. 23.

The theoretical curve is essentially linear when

$$\frac{r_o^2 \tau}{D} > \frac{9\tau^2}{4}$$

corresponding to r_o equal to 0.1 cm at a pressure of 11.8 mm of Hg. The experimental curve gives a fair fit with the theoretical curve lending credence to the hypothesis that the secondary peak results from the collision of metastable atoms with the walls. The difference in slope may be due to the fact that the theoretical treatment is based on a constricted discharge of zero radius whereas the discharge radius was actually 0.13 cm.

If δt represents the time after the end of the current pulse at which the secondary light peak occurs then from above

$$\delta t = -\frac{3\tau}{4} + \frac{1}{2}\sqrt{\frac{9\tau^2}{4} + \frac{r_o^2 \tau}{D}}$$

CALCULATED AND EXPERIMENTAL VALUES OF TIME OF SECONDARY LIGHT PEAK AS A FUNCTION OF DISTANCE FROM CONSTRICTED DISCHARGE TO THE WALL

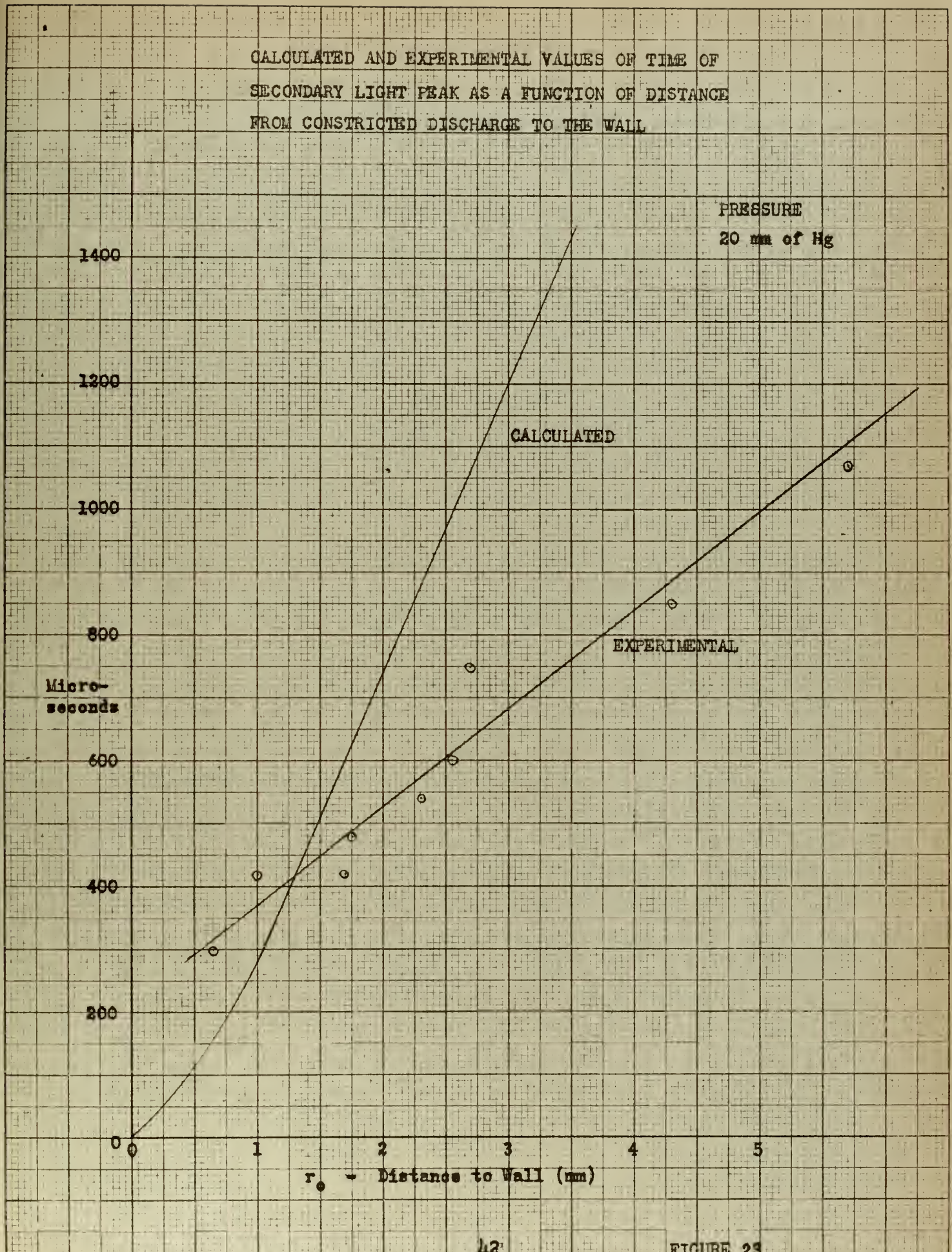

FIGURE 23

where

$$\gamma = \frac{2 \times 10^5 \text{ Collisions/metastable removal}}{\text{Collision frequency}}$$

The collision frequency is

$$Z = \sigma \bar{v} n$$
$$Z = 0.45 \times 10^8 p \quad \text{at } 300^\circ K$$

The diffusion constant D is

$$D = D_o \frac{p_o}{p} = \frac{44.8}{p} \text{ cm}^2/\text{sec}$$

For r_o equal to 0.35 cm

$$\delta t = -\frac{3.3}{p} + \frac{1}{2}\sqrt{\frac{44}{p} + 12.1} \text{ ms}$$

A plot of this function appears on Fig. 24. The distance of the constricted discharge from the wall was set at 0.35 cm, as measured by a cathometer, by application of a small magnetic field, and δt was measured on the oscilloscope. This procedure was repeated at several pressures between 2 and 20 mm of Hg. Experimental values for δt plotted on Fig. 24 show that the theoretical treatment was essentially correct.

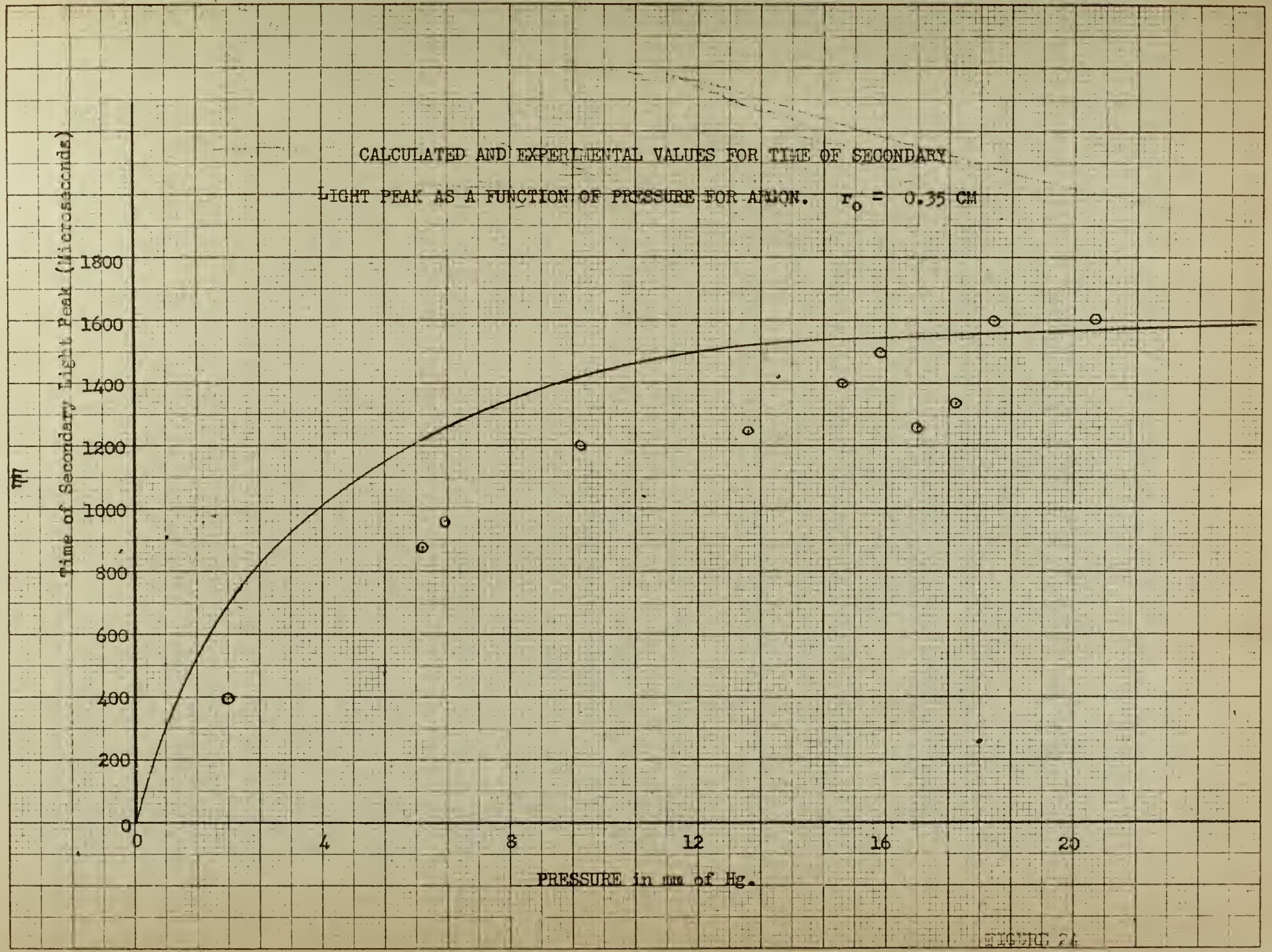
CALCULATED AND EXPERIMENTAL VALUES FOR TIME OF SECONDARY
LIGHT PEAK AS A FUNCTION OF PRESSURE FOR ARGON. r_0 = 0.35 CM
Time of Secondary Light Peak (Microseconds)
1800
1600
1400
1200
1000
800
600
400
200
0
0
4
8
12
16
20
PRESSURE in mm of Hg.

FIGURE 24

VI

CONCLUSIONS

The anomalous mode in argon at pressures between 2 and 20 mm of Hg was found to have these characteristics:

1. The frequency of oscillation is a function of the circuit RC product which decreases with increasing RC. It is a linear function of the average tube current.

2. The voltage waveform degenerates from a sinusoid at very low RC products to a sawtooth throughout most of the range of RC.

3. The discharge tube exhibited negative dynamic resistance throughout the anomalous mode.

4. The frequency decreased with increasing argon pressure.

5. As the voltage waveform degenerated into a sawtooth, the current wave form became a short pulse of great amplitude. Current pulses of about 10 microsecond duration and of several amperes amplitude were obtained at values of average current in the range of 0.5 to 25 milliamperes.

6. Peak current amplitude and percentage modulation of the voltage across the tube increased with increasing RC product.

The light intensity in the afterglow in an argon discharge increased to a maximum about 100 microseconds after the excitation was removed and then decayed. This 100 microsecond delay appeared to be invariant with change in any of the discharge parameters. The decay of the light appeared to follow those processes formulated by other investigators in this field. Identification of the separate processes is theorized only due to the lack of a means of measuring electron density directly as a function of time. With an assumed value of 3×10^{-7} cm^3/ion-sec for the recombination coef-

ficient, electron densities of the order of $10^9/cm^3$ and characteristic calculated decay times of the order of 10^{-4} seconds were obtained, both in good agreement with reported values [4,6].

A secondary light peak occurred during the later stages of light decay. It is believed that this phenomenon can be attributed to metastable recombination near the walls. Perhaps the electrons have "cooled" sufficiently in the time necessary for the metastables to diffuse to the walls so that this reaction can take place with a high probability in that region according to

$$A^M + e^- \rightarrow A^*$$

$$A^* \rightarrow A + h\nu$$

BIBLIOGRAPHY

1. MCDONNEL, J. L. and SHERMAN, R. O., Striations in the Positive Column of an Argon Glow Discharge, Thesis, U. S. Naval Postgraduate School, Monterey, California (1958). Unpublished.

2. ALPERT, D., New Developments in the Production and Measurement of Ultra High Vacuum, JOUR. OF APPL. PHYS. 24, 860 (1953).

3. GILL, E. W. B., PHIL. MAG. 8, 955 (1929).

4. REDFIELD, A. and HOLT, R. B., Electron Removal in Argon Afterglows, PHYS. REV. 82, 874 (1951).

5. OLSEN, H. N. and HUXFORD, W. S., Dynamic Characteristics of Plasma, PHYS. REV. 87, 927 (1952).

6. GOLDSTEIN, L., Gaseous Electronics, ELECTRONICS AND ELECTRON PHYSICS, p 473.

7. GOLDSTEIN, L., Gaseous Electronics, ELECTRONICS AND ELECTRON PHYSICS, p 453.

8. BIONDI, M. A. AND BROWN, C. S., Measurement of Electron-Ion Recombination, PHYS. REV. 76, 1697 (1949).

9. KENTY, C., Recombination of Argon Ions and Electrons, PHYS. REV., 32, 624 (1928).

10. JOHNSON, E. O. and MALTER, L., PHYS. REV., 80, 58 (1950).

11. BATES, D. R., PHYS. REV., 77, 718 (1950).

12. BIONDI, M. A. PHYS. REV., 83, 1079 (1950).

13. MITCHELL, A. C. G. and ZEMANSKY, M. W., RESONANCE RADIATION AND EXCITED ATOMS, p 246 (1934).

14. COLLI, L., GATTI, E., and FACCHINI, U., PHYS. REV. 80, 92 (1950); COLLI, L., PHYS. REV., 95, 892 (1954); COLLI, L., and FUCCHINI, U., PHYS. REV. 96, 1 (1954).

15. LOEB, L. B., BASIC PROCESSES OF GASEOUS ELECTRONICS, p 879 (1955).

16. LOEB, L. B., BASIC PROCESSES OF GASEOUS ELECTRONICS, p 199 (1955).